



Full length article



## Di-(2-ethylhexyl) phthalate substitutes accelerate human adipogenesis through PPAR $\gamma$ activation and cause oxidative stress and impaired metabolic homeostasis in mature adipocytes

Alexandra Schaffert<sup>a</sup>, Isabel Karkossa<sup>a</sup>, Elke Ueberham<sup>b</sup>, Rita Schlichting<sup>c</sup>, Katharina Walter<sup>a</sup>, Josi Arnold<sup>a</sup>, Matthias Blüher<sup>d,e</sup>, John T. Heiker<sup>d</sup>, Jörg Lehmann<sup>f,g</sup>, Martin Wabitsch<sup>h</sup>, Beate I. Escher<sup>c,i</sup>, Martin von Bergen<sup>a,j,k</sup>, Kristin Schubert<sup>a,\*</sup>

<sup>a</sup> Department of Molecular Systems Biology, Helmholtz Centre for Environmental Research (UFZ), Leipzig, Germany

<sup>b</sup> Department of GMP Process Development / ATMP Design, Fraunhofer Institute for Cell Therapy and Immunology, Leipzig, Germany

<sup>c</sup> Department of Cell Toxicology, Helmholtz Centre for Environmental Research (UFZ), Leipzig, Germany

<sup>d</sup> Helmholtz Institute for Metabolic, Obesity and Vascular Research (HI-MAG), Leipzig, Germany

<sup>e</sup> Department of Endocrinology, Nephrology and Rheumatology, Faculty of Medicine, University of Leipzig, Leipzig, Germany

<sup>f</sup> Department of Preclinical Development and Validation, Fraunhofer Institute for Cell Therapy and Immunology, Leipzig, Germany

<sup>g</sup> Fraunhofer Cluster of Excellence Immune-Mediated Diseases CIMD, Fraunhofer Institute for Cell Therapy and Immunology, Leipzig, Germany

<sup>h</sup> Division of Pediatric Endocrinology and Diabetes, Ulm University Medical Center, Ulm, Germany

<sup>i</sup> Environmental Toxicology, Center for Applied Geoscience, Eberhard Karls University Tübingen, Germany

<sup>j</sup> Institute of Biochemistry, Leipzig University, Leipzig, Germany

<sup>k</sup> German Centre for Integrative Biodiversity Research (iDiv) Halle-Jena-Leipzig, Leipzig, Germany

### ARTICLE INFO

Handling Editor: Adrian Covaci

#### Keywords:

Peroxisome proliferator-activated receptor  $\gamma$  (PPAR $\gamma$ )

Plasticizers

Endocrine disruption

Oxidative stress

SGBS

Proteomics

### ABSTRACT

The obesity pandemic is presumed to be accelerated by endocrine disruptors such as phthalate-plasticizers, which interfere with adipose tissue function. With the restriction of the plasticizer di-(2-ethylhexyl)-phthalate (DEHP), the search for safe substitutes gained importance. Focusing on the master regulator of adipogenesis and adipose tissue functionality, the peroxisome proliferator-activated receptor gamma (PPAR $\gamma$ ), we evaluated 20 alternative plasticizers as well as their metabolites for binding to and activation of PPAR $\gamma$  and assessed effects on adipocyte lipid accumulation. Among several compounds that showed interaction with PPAR $\gamma$ , the metabolites MINCH, MHINP, and OH-MPHP of the plasticizers DINCH, DINP, and DPHP exerted the highest adipogenic potential in human adipocytes. These metabolites and their parent plasticizers were further analyzed in human preadipocytes and mature adipocytes using cellular assays and global proteomics. In preadipocytes, the plasticizer metabolites significantly increased lipid accumulation, enhanced leptin and adiponin secretion, and up-regulated adipogenesis-associated markers and pathways, in a similar pattern to the PPAR $\gamma$  agonist rosiglitazone. Proteomics of mature adipocytes revealed that both, the plasticizers and their metabolites, induced oxidative stress, disturbed lipid storage, impaired metabolic homeostasis, and led to proinflammatory and insulin resistance promoting adipokine secretion. In conclusion, the plasticizer metabolites enhanced preadipocyte differentiation, at least partly mediated by PPAR $\gamma$  activation and, together with their parent plasticizers, affected the functionality of mature adipocytes similar to reported effects of a high-fat diet. This highlights the need to further investigate the currently used plasticizer alternatives for potential associations with obesity and the metabolic syndrome.

### 1. Introduction

The obesity pandemic contributes to higher mortality, mainly by increasing the risk of cardiovascular diseases, type 2 diabetes, fatty liver

disease, and certain types of cancer (Abdelaal et al., 2017). While genetic predisposition, a hypercaloric and palatable food environment, and a sedentary lifestyle are major contributing factors, endocrine disruptive chemicals such as plasticizers promote and accelerate adipose

\* Corresponding author at: Department of Molecular Systems Biology, Helmholtz Center for Environmental Research, Permoserstraße 15, 04318 Leipzig, Germany.  
E-mail address: [kristin.schubert@ufz.de](mailto:kristin.schubert@ufz.de) (K. Schubert).

<https://doi.org/10.1016/j.envint.2022.107279>

Received 7 February 2022; Received in revised form 8 April 2022; Accepted 2 May 2022

Available online 6 May 2022

0160-4120/© 2022 The Authors. Published by Elsevier Ltd. This is an open access article under the CC BY-NC-ND license (<http://creativecommons.org/licenses/by-nc-nd/4.0/>).

tissue dysfunction and increase the prevalence of obesity-related comorbidities (Abdelal et al., 2017; Muscogiuri et al., 2017).

Plasticizers are used in plastic products such as polyvinyl chloride (PVC), food and beverage packaging, medical items, children's toys, and face masks (Hahladakis et al., 2018; Xie et al., 2022). Unfortunately, plasticizers can easily migrate from the material to the surrounding environment or to children handling the plastic product (Benjamin et al., 2017). In consequence, plasticizers and their metabolites have been detected in human urine (Silva et al., 2007), blood (Hogberg et al., 2008; Specht et al., 2014), and breast milk (Hogberg et al., 2008). Besides impairing fertility, fetal development, immune response, and accelerating cancer development, a recent meta-analysis of epidemiological evidence has shown that increased exposure to phthalates is consistently associated with obesity in children and adults (Ribeiro et al., 2020). Additionally, numerous *in vivo* studies have demonstrated a direct link between plasticizer exposure and obesity outcomes (Le Magueresse-Battistoni et al., 2017). The previously most commonly used plasticizer di-(2-ethylhexyl)-phthalate (DEHP) was observed to cause weight gain in female mice, alter adipokine concentrations in blood, and impair insulin tolerance (Hao et al., 2012; Klötting et al., 2015; Schmidt et al., 2012). As an underlying cause, the endocrine functions of the white adipose tissue in particular have been proven to be disturbed by phthalates (Darbre, 2017).

Adipose tissue is recognized as an important endocrine organ that secretes a multitude of signaling molecules (adipokines) and regulates energy homeostasis, immune responses, as well as cardiovascular functions (Rosen and Spiegelman, 2014). The peroxisome-proliferator-activated receptor  $\gamma$  (PPAR $\gamma$ ) is highly expressed in adipose tissue and is considered a key regulator of adipocyte differentiation, as well as lipid metabolism, inflammation, insulin sensitivity, and glucose homeostasis (Neels and Grimaldi, 2014). Mechanistically, PPAR $\gamma$  controls the expression of key adipokines such as leptin and adiponectin, which regulate satiety, inflammation, and insulin sensitivity (Harris, 2014; Hoffstedt et al., 2004). Many *in vitro* studies have demonstrated an increase of adipocyte differentiation and lipid accumulation by the DEHP metabolite mono-(2-ethylhexyl) phthalate (MEHP) in 3T3-L1 mouse adipocytes (Feige et al., 2007; Hurst and Waxman, 2003; Qi et al., 2019). Several studies indicate that these adipogenic properties might be caused by PPAR $\gamma$  activation (Feige et al., 2007; Hurst and Waxman, 2003; Kratochvil et al., 2018).

Because of their endocrine disruptive effects, DEHP and other low molecular weight phthalates were classified as substances of very high concern (SVHC) in the European Chemicals Regulation REACH by the European Chemicals Agency (ECHA) (EP 2006; ECHA 2018). In the US, the Consumer Product Safety Improvement Act of 2008 prohibits the presence of three phthalates, among them DEHP, in children's toys ('The Consumer Product Safety Improvement Act (CPSIA)'). Alternatives replacing DEHP in consumer-related products are primarily high molecular weight phthalates diisononyl phthalate (DINP), diisodecyl phthalate (DIDP), and di-(2-propylheptyl) phthalate (DPHP), and some non-phthalate plasticizers such as 1,2-cyclohexanedioic acid diisononyl ester (DINCH), dioctyl terephthalate (DOTP/DEHT), and acetyl tributyl citrate (ATBC) (Nagorka and Koschorreck, 2020; Van Vliet et al., 2011). Still, missing data on potential adipogenic effects of these compounds creates a high level of uncertainty on their suitability as safe substitutes. In addition to that, the underlying mode of action of the adipogenic properties of plasticizers in general is not fully understood due to the lack of systems biology approaches (Lind et al., 2012; Stahlhut et al., 2007). Furthermore, while the majority of studies solely investigated the aspect of adipogenesis promotion by plastic additives in preadipocytes, there is a need to investigate the impact of these compounds on differentiated, mature adipocytes.

Thus, the primary aim of this study was to analyze the PPAR $\gamma$ -mediated effects of plasticizers and their metabolites in human adipocytes and uncover the underlying mode of action. In contrast to the frequently used mouse 3T3-L1 cells, and the assessment of only a few

compounds we screened 20 compounds, including poorly characterized emerging substitutes, in the human SGBS adipocyte model. We used a global proteomics approach to reveal detailed mechanistic insights into the modes of action of the most potent compounds during human preadipocyte differentiation and on mature human adipocytes.

## 2. Materials and methods

20 plasticizers and their metabolites were purchased from the suppliers listed in Supplement 1, Table S1.

### 2.1. Surface plasmon resonance (SPR) spectroscopy

SPR was previously used to determine binding efficacies of various ligands to human PPAR $\gamma$  (Shang and Kojetin, 2021; van Marrewijk et al., 2016; Yu et al., 2004), including the binding of xenobiotics (Kratochvil et al., 2018; Schaffert, Krieg, et al., 2021).

All 20 analytes were screened on a Biacore T200 instrument (GE Healthcare, Freiburg, Germany) as described previously (Schaffert, Krieg, et al. 2021). In brief, the surface of an S Series Sensor Chip CM5 (GE Healthcare, Freiburg, Germany) was activated for immobilization with a mixture containing 50 mM N-hydroxysuccinimide (NHS) and 195.6 mM 1-ethyl-3-(3-dimethylaminopropyl) carbodiimide hydrochloride (EDC). A recombinant human PPAR $\gamma$  ligand-binding domain (LBD) (Biozol, Eching, Germany) was immobilized on the chip surface at 25 °C via amine coupling and using a protein concentration of 80  $\mu$ g/ml in 10 mM sodium acetate buffer (pH 4.5) at a flow rate of 5  $\mu$ l/min according to the manufacturer's protocol, leading to immobilization of 8959.4 RU and 9530.4 RU on two sensor chips. Unreacted NHS-esters were deactivated by 1 M ethanolamine-HCl (pH 8.5). All analyses were conducted using a buffer containing phosphate-buffered saline (PBS, GE Healthcare, Freiburg, Germany) and uniform amounts of DMSO (3%) or MeOH (1%), depending on the solvent in which the compounds were dissolved. The signal of a chemically inactivated, empty reference flow cell was subtracted from response signals of the cell loaded with the PPAR $\gamma$  LBD to adjust for unspecific binding to the surface. Measurements were conducted at least in triplicate for every analyte. Raw relative responses (Supplement 2) were normalized to the analyte's molecular weight (MW, Supplement 1, Table S1) by RU/MW\*100. The signal was subsequently normalized to the corresponding highest concentration of the endogenous PPAR $\gamma$  ligand 15-deoxy- $\delta$ 12,14-prostaglandin J2 (15d-PGJ2), that was used as positive control in every run (Supplement 3). The mean value derived from three buffer injections, subsequently to four start-up injections, was used as negative control.

### 2.2. Reporter gene assay

The ability of the plasticizers to effectively activate PPAR $\gamma$  was tested using the GeneBLazer® PPAR $\gamma$ -UAS-bla 293HEK cell-based reporter gene assay (Thermo Fisher Scientific, Waltham, MA, USA). PPAR $\gamma$  activation was quantified in parallel with cell viability as described previously (König et al., 2017; Schaffert, Krieg, et al., 2021). Briefly, after seeding in 384-well plates at 6000 cells/well using 30  $\mu$ l assay medium (phenol-red free DMEM, 2% charcoal treated fetal bovine serum, 100 U/ l penicillin, and 0.1 mg/l streptomycin), cells were incubated for 24 h at 37 °C with 5% CO<sub>2</sub> in 95% humidity. 10  $\mu$ l assay medium containing rosiglitazone, which served as a positive control, or test compounds in serial or linear dilutions were then added and incubated for 22 h at 37 °C with 5% CO<sub>2</sub> in 95% humidity. Compounds were dissolved in DMSO or MeOH. After the addition of 8  $\mu$ l FRET detection reagent with ToxBlazer mixture, blue and green fluorescence signals were read using a 409 nm excitation filter at 460 nm and 520 nm for potential autofluorescence and again after 2 h at room temperature. PPAR $\gamma$  activation was determined by the ratio of blue to green FRET fluorescence signal. The signal was converted to % effect by adjusting

unexposed cells that were not treated with chemical or solvent to 0% activation and the maximum effect by rosiglitazone to 100% activation. It was verified that the solvent concentrations used for the test compounds did not impact the assay. For this, serial dilutions of DMSO and MeOH stocks were assayed and found to reduce cell viability by 10% (IC<sub>10</sub>) at 5.96% (v/v) (MeOH) and 1.1% (v/v) (DMSO). There was no detectable effect on the reporter gene beta-lactamase activation in the GeneBLAZer® assay at the applied solvent concentrations (maximum of 0.05% (v/v) for DMSO and 0.5% (v/v) for MeOH).

Cell viability was calculated using cell confluency detected via an IncuCyte S3 live cell imaging system (Essen BioScience, Ann Arbor, Michigan, USA) as described before (Escher et al., 2019). The inhibitory concentration for 10% reduction of cell viability (IC<sub>10</sub>) was determined in GraphPad Prism 8, and only compound concentrations below the IC<sub>10</sub> were included in the evaluation of PPAR $\gamma$  activation. Experiments for analytes that showed activation were carried out in four independent replicates. Experiments for analytes that showed no activation were conducted in duplicates.

### 2.3. SGBS cell culture

Because of their similarity to differentiated human primary preadipocytes (Wabitsch et al., 2001), differentiated human preadipocytes of the Simpson-Golabi-Behmel syndrome (SGBS) cell strain were used as a model system to investigate the cellular mode of action of a variety of plasticizers in human adipocytes. SGBS cells were obtained from the laboratory of Prof. Dr. Martin Wabitsch and differentiated according to the standard protocol as described previously (Wabitsch et al., 2001). In brief, cells were cultured at 5% CO<sub>2</sub> and 37 °C in 95% humidity. SGBS preadipocytes of generation 40 and passage 3 after thawing were grown to complete confluence with DMEM/F12 containing 33  $\mu$ M biotin, 17  $\mu$ M pantothenate, 100 U/l penicillin, and 0.1 mg/l streptomycin (basal medium) supplemented with 10% FCS (Gibco, Carlsbad, CA, USA). According to the standard differentiation protocol, differentiation of the confluent cells was initiated (day 0) after changing to serum-free basal medium supplemented with 0.1  $\mu$ M cortisol, 0.01 mg/ml apotransferrin, 0.2 nM triiodothyronine, and 20 nM human insulin (differentiation medium) with the addition of 2  $\mu$ M rosiglitazone, 25 nM dexamethasone, and 200  $\mu$ M 3-isobutyl-1-methylxanthine for the first four days.

For investigation of effects on preadipocytes, the positive control was differentiated using the standard protocol with rosiglitazone. For plasticizer treatments, differentiation was conducted without rosiglitazone and cells were continuously exposed from day 0 – day 16 to the plasticizers or their metabolites. As for plasticizer treatments, the negative control was differentiated with rosiglitazone-free medium containing equivalent amounts of solvent (0.01% MeOH, v/v) for 16 days, resulting in minimal differentiation. All media were renewed every second day to mimic continuous exposure.

For investigation of effects in mature adipocytes, SGBS cells were first differentiated according to the described standard protocol for 12 days using rosiglitazone in the first four days. Obtained mature adipocytes were then exposed to the plasticizers for 8 days with medium changes every second day. The control contained equivalent amounts of solvent. All SGBS cell culture experiments were conducted in quadruplicate.

### 2.4. DAPI and Nile Red staining

To assess cell viability and simultaneous lipid quantification, SGBS cells were stained with 4', 6-diamidino-2-phenylindole, dihydrochloride (DAPI, Sigma-Aldrich, Taufkirchen, Germany), and Nile Red (Sigma-Aldrich, Taufkirchen, Germany) according to Aldridge et al. (2013). Briefly, SGBS cells were grown in a 96-well plate as described in 2.4, preserved with 4% paraformaldehyde (Sigma-Aldrich, Taufkirchen, Germany) in PBS (Lonza, Basel, Switzerland) for 15 min at room

temperature. The cells were washed with PBS and background fluorescence was read at Ex 360/Em 480 for DAPI and Ex 485/Em 530 for Nile Red in a 5  $\times$  5 spot pattern. The cells were stained with 100  $\mu$ l 0.2% saponin, 1  $\mu$ g/ml DAPI, and 1  $\mu$ g/ml Nile Red in PBS for 15 min. After washing three times with PBS, the fluorescence was read as before. Experiments were performed in quadruplicate. The background fluorescence was subtracted for each well, and average intensities were calculated. For cell viability, the ratio of DAPI staining values of treated cells to the vehicle control was used. To quantify lipid accumulation, the ratio of Nile Red to DAPI stained cells was calculated, and treatments were compared to the vehicle control.

### 2.5. Adipokine ELISAs

Adipokines leptin, adiponectin, and CC-chemokine ligand 2 (CCL2/MCP-1) were quantified in SGBS cell culture supernatants using DuoSet ELISA kits from R&D Systems (Minneapolis, MN, USA) according to the manufacturer's instructions. To account for differences in cell number, adipokine levels were normalized to DAPI.

### 2.6. Statistical analysis

With the exception of the proteomics data, all data are described as means  $\pm$  standard deviation (SD) and analyzed by one-way ANOVA, either correcting for multiple testing by Dunnett's posthoc tests or uncorrected as Fisher's LSD posthoc tests using the GraphPad 8 software (GraphPad Software Inc., La Jolla, CA, USA).

### 2.7. Proteomics sample preparation

After growth and treatment in 12-well plates, SGBS cells were washed once with 3 ml ice-cold PBS and harvested with lysis buffer containing 150 mM NaCl, 1% Triton X-100, 50 mM Tris HCl pH 7.4, 0.5% sodium deoxycholate, and 0.1% sodium dodecyl sulfate in ddH<sub>2</sub>O supplemented with complete Roche protease inhibitor (Sigma-Aldrich, Taufkirchen, Germany). Lysates were incubated for 1 h on ice and centrifuged for 15 min at 4 °C and 16,000  $\times$  g. Protein concentration was determined by Pierce BCA assay (Thermo Fisher Scientific, Waltham, MA, USA) according to the manufacturer's instructions.

Samples were prepared by single-pot solid-phase-enhanced sample preparation (SP3) in combination with a tandem mass tag (TMT) labeling strategy (TMT-16-plex for the dataset of the preadipocytes and TMT-10-plex for the dataset of mature adipocytes) for protein quantification because we previously demonstrated this allows to robustly identify pathways in a toxicological context (Bannuscher et al., 2020; Hughes et al., 2014; Hughes et al., 2019; Wang, Karkossa, et al. 2020). Samples were prepared as described before (Schaffert, Arnold, et al. 2021), except that 15  $\mu$ M protein per sample was used and acidification for binding to the magnetic beads was not applied.

### 2.8. Proteomics using LC-MS/MS

Obtained peptides were separated using an Ultimate 3000 nano ultra-performance liquid chromatography system (Thermo Fisher Scientific, Waltham, MA, USA) as described before (Wang, Karkossa, et al. 2020). Samples were first trapped on an Acclaim PepMap 100 C18 column, nanoViper, 2  $\mu$ m, 75  $\mu$ m  $\times$  5 cm column (Thermo Fisher Scientific, Waltham, MA, USA) and subsequently separated on an analytical reverse-phase column Acclaim PepMap 100 C18, nanoViper, 3  $\mu$ m, 75  $\mu$ m  $\times$  25 cm column (Thermo Fisher Scientific, Waltham, MA, USA) using a non-linear gradient of a hydrophilic solution (0.1% FA in H<sub>2</sub>O, v/v) and a hydrophobic solution (80% ACN, 0.1% FA in H<sub>2</sub>O, v/v) at a flow rate of 0.3  $\mu$ l/min. The separated peptides were injected into a Q Exactive HF Hybrid Quadrupole Orbitrap mass spectrometer (Thermo Fisher Scientific, Waltham, MA, USA) equipped with a TriVersa Nano-Mate system (Advion, Ithaca, NY USA). The samples were analyzed

using mass spectrometry parameters as previously described, except for selecting the top 15 precursor ions of each MS1 scan for fragmentation (Wang, Karkossa, et al. 2020). Raw data were processed using Proteome Discoverer (2.5.0.400, Thermo Fisher Scientific, Waltham, MA, USA). The database search was performed using the UniprotKB/Swissprot reference proteome of Homo sapiens (3 May 2020). The analysis resulted in replicate-wise TMT-reporter ion intensity fold changes (FCs) of treatment vs. vehicle control (preadipocyte dataset: Supplement 4; mature adipocyte dataset: Supplement 5) which were used for subsequent analyses. Mass spectrometry data were deposited to the ProteomeXchange Consortium via the PRIDE (Perez-Riverol et al., 2019) partner repository with the dataset identifier PXD031041 and <https://doi.org/10.6019/PXD031041> for the preadipocyte dataset and identifier PXD030843 and <https://doi.org/10.6019/PXD030843> for the mature adipocyte dataset.

## 2.9. Analysis of proteomics data

MS data were statistically analyzed with R v3.6.1 using the packages plyr (Wickham, 2011), reshape2 (Wickham, 2007), xlsx (Dragulescu, 2020), DEP (Zhang et al., 2018), ggsci (Xiao, 2018), circlize (Gu et al., 2014), calibrate (Graffelman, 2005), ggplot2 (Wickham, 2016), readxl (Wickham, 2019b), qpcR (Spiess A., 2018), splitstackshape (Mahto, 2019), tidyr (Wickham, 2019a), and Tmisc (Turner, 2019). Protein FCs were first log2-transformed and then filtered for proteins quantified in at least three of four replicates. Significantly altered proteins between treatments and control were calculated with Student's t-tests (preadipocyte dataset: Supplement 6; the mature adipocyte dataset: Supplement 7).

Significantly changed proteins ( $p \leq 0.05$ ) were matched to pathways using Ingenuity Pathway Analysis software (IPA, QIAGEN Bioinformatics, Hilden, Germany). Parameters such as "human", "adipocytes", "adipose tissue", and "3T3L1 cell line" were defined. Pathways were considered significantly enriched with Benjamini and Hochberg-adjusted  $p$ -value  $\leq 0.05$  (preadipocyte dataset: Supplement 8; mature adipocyte dataset: Supplement 9). Given z-scores represent activation ( $z$ -score  $> 0$ ) or inhibition ( $z$ -score  $< 0$ ) of the pathway. Furthermore, upstream regulators (Supplement 10), as well as diseases and functions (Supplement 11), were extracted from IPA for the preadipocyte dataset.

Using R v3.4.0, normalized and filtered protein  $\log_2$ (FCs) were subjected to Weighted Gene Correlation Analysis (WGCNA) (Langfelder and Horvath 2008, 2012). Networks with 7 modules (preadipocytes dataset) and 6 modules (mature adipocytes dataset) were created applying the default parameters with the following exceptions: soft power threshold: 7, minimum module size: 50, maximum module size: 200, deep split: 1, merge cut height: 0.1. Modules were correlated to traits using Pearson correlation and Student asymptotic  $p$ -values. The trait matrices included compounds, time points, and concentrations (preadipocyte dataset: Supplement 12; mature adipocyte dataset: Supplement 13). For module-trait combinations which were of further interest, key drivers were obtained with gene significance and module membership  $\geq 0.7$  (preadipocyte dataset: Supplement 14; mature adipocyte dataset: Supplement 15) and top 10 key drivers were selected based on summed absolute gene significance and module membership (preadipocyte dataset: Supplement 16; mature adipocyte dataset: Supplement 17). KEGG enrichment for identified key drivers was performed with Cytoscape (v3.9.0) using ClueGo (v2.5.5) and a minimum cluster size of 3 genes, minimum 3% genes per term, pathway network connectivity of 0.4, and otherwise default settings.

## 3. Results

### 3.1. Screening for PPAR $\gamma$ interactions and induction of adipogenesis

The transcription factor PPAR $\gamma$  plays a pivotal role in the regulation of adipocyte function and preadipocyte differentiation (Lefterova et al.,

2014). To identify potential endocrine disruptors acting through direct interaction with PPAR $\gamma$ , we determined molecular binding of 20 plasticizers and selected metabolites to PPAR $\gamma$  by Surface Plasmon Resonance Spectroscopy (SPR). We investigated compounds used as DEHP substitutes, including high molecular weight phthalates (DINP, DIDP, DPHP) and non-phthalate plasticizers (DINCH, ATBC, DOTP) (Nagorka and Koschorreck, 2020; Van Vliet et al., 2011). Plasticizers are rapidly metabolized (Frederiksen et al., 2007) and their metabolites were shown to be more bioactive, thus, investigating biological effects of plasticizer metabolites is of vital importance. Similar to the naturally occurring PPAR $\gamma$  agonist 15d-PGJ2, several compounds showed significant binding to the human recombinant PPAR $\gamma$  LBD in a concentration-dependent manner, including parent plasticizers and metabolites (Fig. 1). Raw and normalized binding signals can be found in Supplement 2.

Subsequent biological activation of PPAR $\gamma$  was quantified by reporter gene activation in the cell-based GeneBLAZER $\text{\textcircled{R}}$  assay and the EC $_{10}$  (concentration at 10% of the maximum effect) was derived from the concentration-effect curves (Supplement 1, Table S2). Only compound concentrations below the IC $_{10}$  (concentration at 10% reduction of cell viability) were included in the evaluation of PPAR $\gamma$  activation. The PPAR $\gamma$  agonist rosiglitazone served as a positive reference and displayed a consistent activation signal (Supplement 1, Fig. S1). 15d-PGJ2 activated PPAR $\gamma$  at an EC $_{10}$  of 65 nM. Several of the plasticizers and their metabolites induced activation of PPAR $\gamma$  with EC $_{10}$  values in the range of 1  $\mu$ M – 10  $\mu$ M (Fig. 1). MINCH slightly activated PPAR $\gamma$  in the reporter gene assay, but an EC $_{10}$  could not be derived due to its low IC $_{10}$  (Supplement 1, Fig. S2). For BBP, MBEP, and MBUP, an IC $_{10}$  was observed, which was clearly above the EC $_{10}$  (Supplement 1, Table S2). Dose-response curves for each activating compound (Fig. S2) and not activating compound (Fig. S3) can be found in Supplement 1. Not all compounds that bound to PPAR $\gamma$ , as revealed by SPR, facilitated PPAR $\gamma$ -activation and vice versa (Fig. 1).

Since differentiation of preadipocytes and lipid accumulation are primary outcomes of PPAR $\gamma$  activation (Lefterova et al., 2014), the impact of plasticizers on lipid accumulation was determined in SGBS cells. SGBS cells are a human preadipocyte cell strain derived from subcutaneous white adipose tissue of an infant with Simpson-Golabi-Behmel syndrome (SGBS) and show high similarity to human preadipocytes in primary culture with the benefit of a longer-lasting differentiation capacity (Fischer-Posovszky et al., 2008; Wabitsch et al., 2001). Lipid accumulation was quantified and normalized to DNA content to account for changes in cell number. A significant increase in lipid accumulation was observed for the metabolites MHINP, MCINP, OH-MPHP, MBEP, MINCH, OH-MINCH, and the plasticizer DIDP (Fig. 1). All compounds that induced lipid accumulation did also activate PPAR $\gamma$  in the reporter gene assay, with the exception of DIDP (Fig. 1).

In summary, several plasticizers and their metabolites were able to bind to PPAR $\gamma$ , to activate it, and to increase lipid accumulation, and thus, potentially are triggering adipogenesis in human preadipocytes. Nevertheless, there are disparities between binding, activation, and induction of lipid accumulation in some cases.

### 3.2. Investigation of adverse effects of the three most potent plasticizer metabolites and their parent plasticizers in human adipocytes

Of the 20 compounds studied, MINCH, MHINP, and OH-MPHP (metabolites of DINCH, DINP, and DPHP) exhibited the highest increase in lipid accumulation and, thus, adipogenic potential. Therefore, these metabolites were selected together with their parent plasticizers to further analyze the underlying mode of action (Fig. 2).

Adverse effects on SGBS preadipocytes during differentiation and mature SGBS adipocytes were examined. Preadipocytes were exposed to the compounds for up to 16 days. Standard SGBS differentiation with the synthetic PPAR $\gamma$  agonist rosiglitazone was used as a reference for the induction of adipogenesis and vehicle treated cells (0.01% MeOH, v/v)

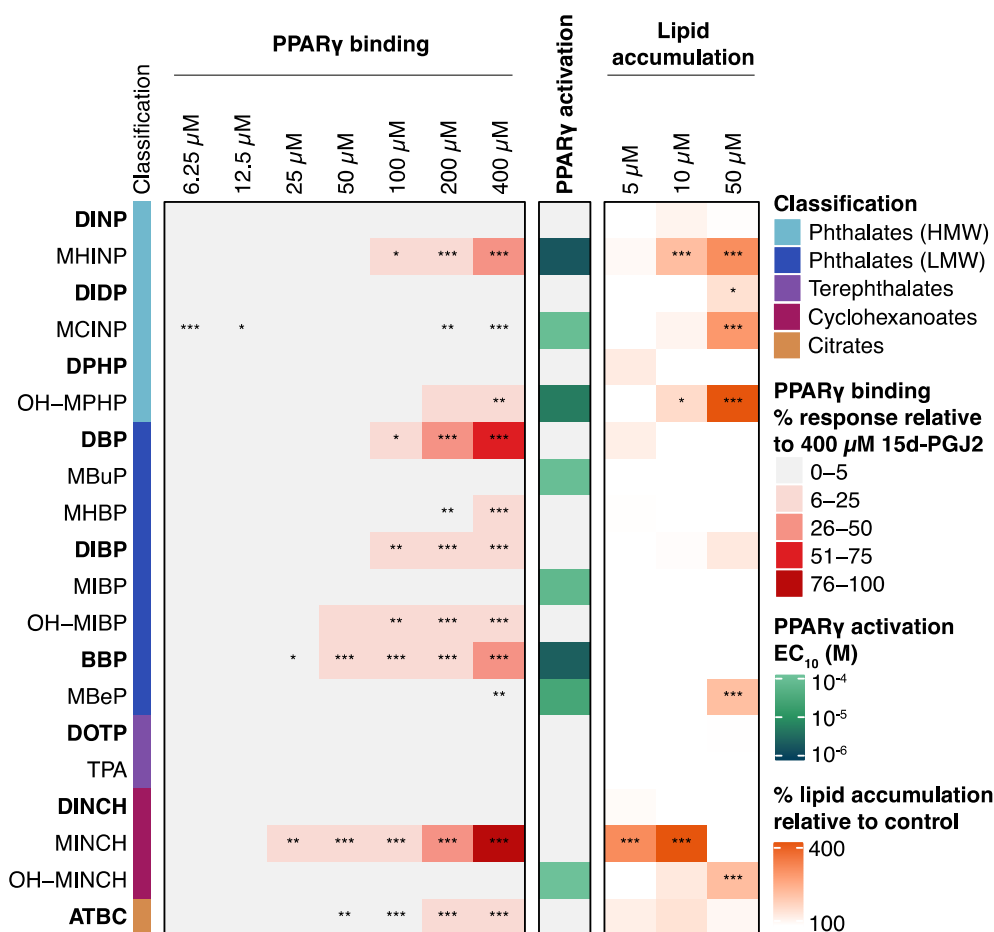


**Fig. 1. Screening of 20 compounds for PPAR $\gamma$  interactions (SPR & reporter gene assay) and induction of adipogenesis in SGBS preadipocytes.** To examine PPAR $\gamma$  binding by SPR, binding responses were normalized to the compounds molecular weight and plotted as a ratio to the natural PPAR $\gamma$  ligand 15d-PGJ2, which served as a positive binding control (100%). Significant changes are indicated with asterisks (\*  $p \leq 0.05$ , \*\*  $p \leq 0.01$ , \*\*\*  $p \leq 0.001$ ,  $n = 3$ ). Parent compounds are displayed in bold with associated metabolites below them. HMW: high molecular weight; LMW: low molecular weight. PPAR $\gamma$  activation was determined by PPAR $\gamma$ -UAS-bla 293H cell-based reporter gene assay and is expressed as EC<sub>10</sub> (10% effect concentration). Effects were observed at non-cytotoxic concentrations. Lipid accumulation was assessed by exposing human SGBS preadipocytes to the compounds for 16 days during differentiation and by normalizing Nile Red staining of the lipids to DAPI staining of DNA content at day 16. The resulting lipid accumulation is shown in comparison to the control containing the same amount of solvent (0.01%, v/v). Significant changes are indicated with asterisks (\*  $p \leq 0.05$ , \*\*  $p \leq 0.01$ , \*\*\*  $p \leq 0.001$ ,  $n = 4$ ). PRINT IN COLOR. (For interpretation of the references to color in this figure legend, the reader is referred to the web version of this article.)

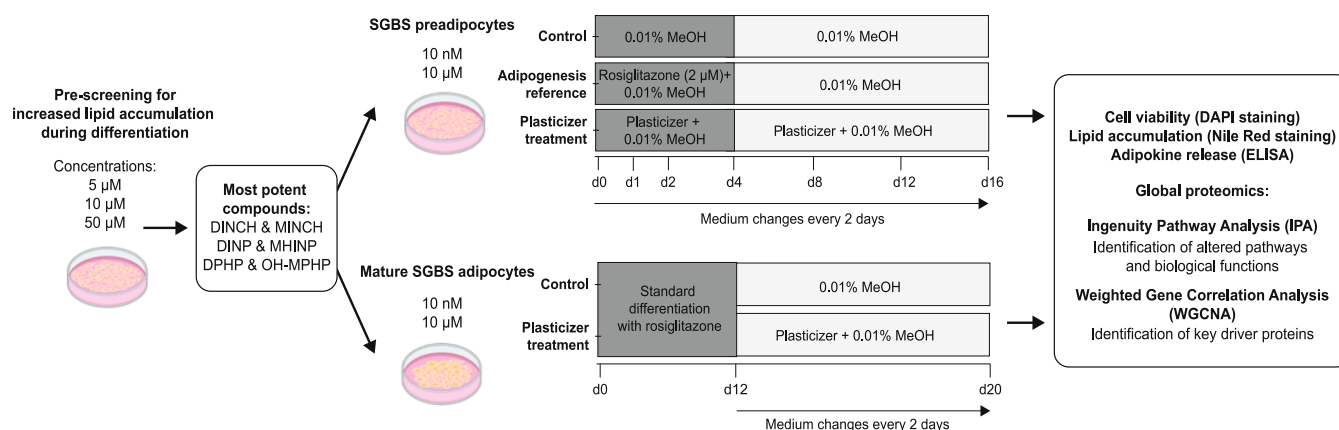


**Fig. 2. Experimental setup for the investigation of plasticizer effects during SGBS preadipocyte and mature SGBS adipocyte exposure.** After screening of 20 compounds, the six most potent plasticizer metabolites and their parent compounds were selected for analysis in SGBS preadipocytes and mature SGBS adipocytes. PRINT IN COLOR.

were used as a negative control.

To study the effects on mature adipocytes, differentiated SGBS cells were treated with the plasticizers and their metabolites for 8 days. To mimic continuous exposure, cell culture media were changed every other day. Cell viability, lipid accumulation, adipokine levels, and proteomic analyses were performed to assess potential adverse effects.

### 3.2.1. Adverse effects during preadipocyte differentiation

To determine the viability of SGBS cells exposed to the selected plasticizers or their metabolites, we quantified DNA content with DAPI

on the last day of exposure (day 16). Among the six compounds, only MINCH showed a decrease in cell viability to ultimately 0% at 100  $\mu\text{M}$ , after a peak maximum of 25  $\mu\text{M}$  (Fig. 3A). DNA content tended to increase for the other compounds, indicating a proliferation effect.

Lipid accumulation was examined for the selected candidates in a broader concentration range, starting at 10 nM, which represents the concentration for plasticizers found in human blood (Specht et al., 2014). In addition to the PPAR $\gamma$  agonist rosiglitazone, the metabolites also showed a significant and concentration-dependent increase in lipid accumulation, with MINCH showing the most substantial effects at 10

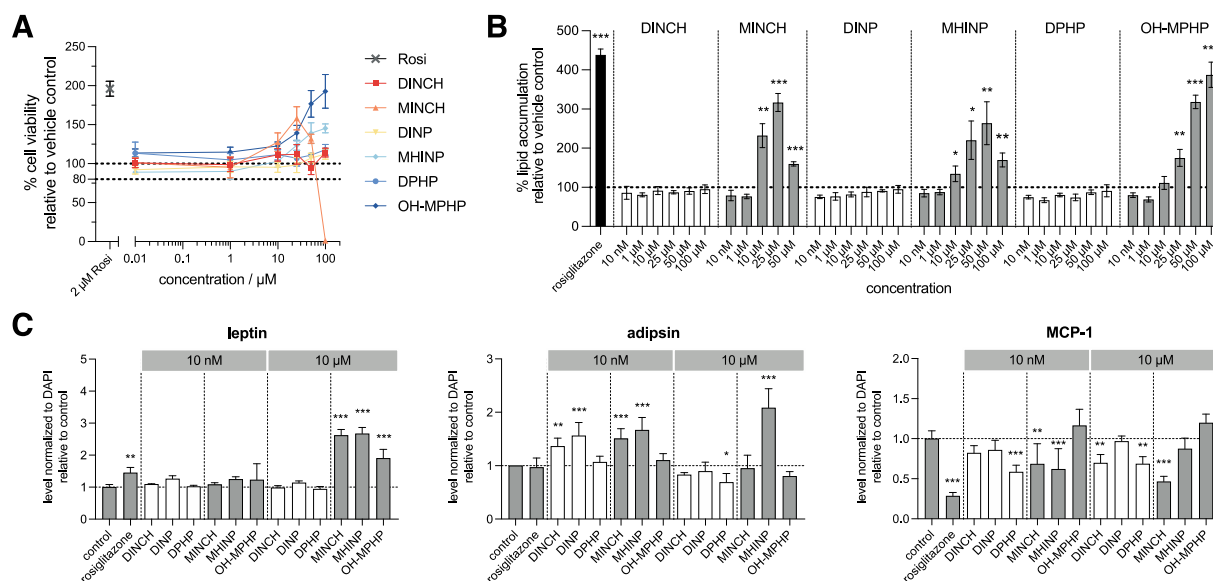


**Fig. 3.** Effect of selected plasticizers and their metabolites on cell viability, lipid accumulation, and adipokine release. Preadipocytes were exposed to the compounds for 16 days during differentiation. The positive control rosiglitazone was applied during the first four days of differentiation according to the standard differentiation protocol. Furthermore, vehicle controls containing equivalent amounts of vehicle solvent were used. (A) Viability of cells relative to the vehicle control was measured by DAPI staining of DNA at day 16. (B) Lipid accumulation relative to the vehicle control were quantified via Nile Red staining at day 16 and normalized to DAPI staining. (C) Levels of adipokines leptin, adipsin, and MCP-1 in cell supernatants relative to the vehicle control at day 16. Significant changes are indicated with asterisks (\*  $p \leq 0.05$ , \*\*  $p \leq 0.01$ , \*\*\*  $p \leq 0.001$ ,  $n = 4$ ). PRINT IN COLOR. (For interpretation of the references to color in this figure legend, the reader is referred to the web version of this article.)

μM, followed by MHINP and OH-MPHP, which slightly increased lipid accumulation at 10 μM and significantly at 25 μM (Fig. 3B). 50 μM MINCH induced lipid accumulation less intensely, probably due to cytotoxic effects. The parent compounds showed no significant effects on lipid accumulation up to a concentration of 100 μM. Notably, MINCH and MHINP showed a similarly effective increase of lipid accumulation in SGBS cells as the DEHP metabolite MEHP which is reported to induce lipid accumulation in 3T3-L1 cells (Feige et al., 2007; Hurst and Waxman, 2003; Qi et al., 2019) (Supplement 1, Fig. S4).

Since a pronounced effect on lipid accumulation was observed at 10 μM for the metabolites, without affecting cell viability, this concentration was chosen as the effective concentration for subsequent analyses and proteomics experiments. In addition, the concentration of 10 nM was included, representing the plasticizer levels found in human blood (Specht et al., 2014).

Adipocytes communicate in an autocrine, paracrine and endocrine manner with surrounding tissues and other organs by releasing adipokines (Rosen and Spiegelman, 2014). Plastic additives have previously been associated with altered secretion of adipokines, contributing to adipose tissue dysfunction (Schaffert, Krieg, et al. 2021; Schaedlich et al., 2018). To test whether the compounds lead to altered adipokine secretion patterns, levels of leptin, adipsin, and CC-chemokine ligand 2 (CCL2/MCP-1) were quantified in the cell culture supernatant of SGBS preadipocytes chronically exposed to 10 nM or 10 μM plasticizers for 16 days. Compared to the control, leptin secretion was significantly increased by rosiglitazone and to a higher degree by the 10 μM concentrations of all three metabolites, which is in line with an induction of adipocyte differentiation and lipid accumulation demonstrated for these candidates (Fig. 3C, Fig. 3B). In addition, both concentrations of DINCH and DINP as well as 10 μM MHINP significantly increased adipsin levels, while 10 μM DPHP resulted in a slight decrease (Fig. 3C). MCP-1 was decreased by rosiglitazone and in part by the compound treatments (Fig. 3C).

In summary, of the selected candidates, only MINCH affected cell viability in the tested range of 10 nM to 100 μM during differentiation of human preadipocytes, beginning at a concentration of 50 μM. The metabolites MINCH, MHINP, and OH-MPHP increased lipid accumulation

concentration-dependently, starting at 10 μM. This was in part reflected by an induction of leptin and adipsin secretion as well as decrease in MCP-1. The concentration of 10 nM, which represents the plasticizer levels found in blood, and the high-effect concentration of 10 μM were selected for further evaluation of adipokine levels revealing an impairment of adipokine secretion.

### 3.2.2. Proteomic analysis of preadipocytes during differentiation

To gain insights into the molecular mode of action of the selected plasticizers and their metabolites on human preadipocytes, LC-MS/MS-based global proteomics was performed.

SGBS preadipocytes were continuously exposed to 10 nM and 10 μM of the plasticizers DINCH, DINP, and DPHP or their metabolites MINCH, MHINP, OH-MPHP for up to 16 days (Fig. 2). For each time point, the compound treatments were compared with a vehicle solvent control (0.01% MeOH, v/v) (Fig. 2). Treatment with the potent PPAR $\gamma$  agonist rosiglitazone served as a positive control. The resulting fold changes (FCs) allowed identification of the primarily plasticizer-induced adipogenic effects.

In total, 2765 proteins were reliably quantified in three of four replicates. The number of significantly ( $p \leq 0.05$ ) altered proteins was highest for the positive control rosiglitazone and increased markedly on day 8 of differentiation (Fig. 4A). Cells treated with 10 μM of plasticizer metabolites showed a significant and time-dependent increase in the number of altered proteins, while the other treatments showed fewer changes.

Enrichment analyses were conducted using IPA. The 10 most affected IPA canonical pathways of every treatment showed major changes for rosiglitazone, including upregulation of a variety of metabolic processes, such as Oxidative Phosphorylation, TCA Cycle, Fatty Acid  $\beta$ -oxidation, and amino acid degradation processes (Fig. 4B). Extracellular matrix (ECM) and proliferation-associated pathways were strongly downregulated by rosiglitazone, starting at day 8 of differentiation. From day 1 to day 4, ECM- and proliferation-associated pathways were slightly upregulated by rosiglitazone and 10 μM of plasticizer metabolites. Overall, MHINP and MINCH showed high similarities to rosiglitazone based on pathway regulation. They also upregulated

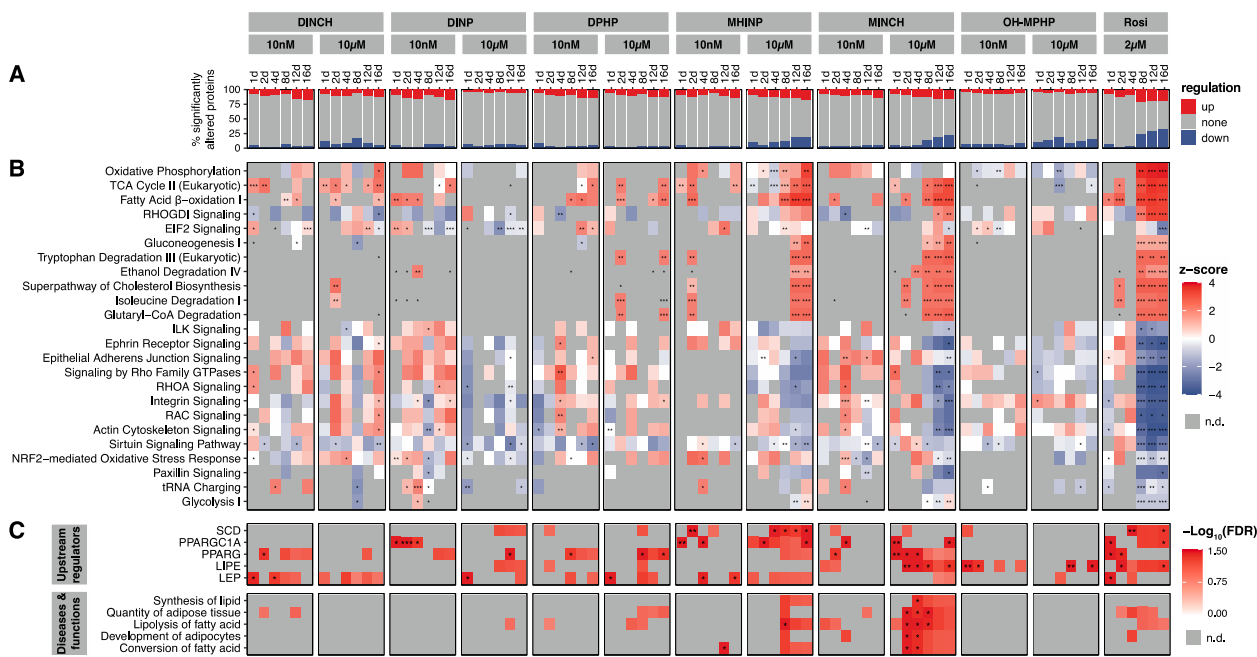


**Fig. 4.** Proteomics analysis after continuous exposure of SGBS preadipocytes to plasticizers and their metabolites during differentiation. Shown are the results obtained by comparison of the compound treatment with the vehicle control (0.01% MeOH, v/v) at the corresponding time point. (A) Percentage of significantly changed proteins ( $p \leq 0.05$ ,  $n = 4$ ). (B) Selection of the top 10 signaling pathways per treatment as obtained from Ingenuity Pathways Analysis (IPA). Heatmap colors are based on z-scores indicating the direction of pathway regulation (z-score  $> 0$  upregulated pathway, z-score  $< 0$  downregulated, grey represents detected score not available). (C) Upstream regulators as well as diseases and functions were enriched via IPA. The level of enrichment is visualized based on the adjusted p-value. Significant changes of pathways, upstream regulators, and functions are indicated with asterisks (\* p.adjusted  $\leq 0.05$ , \*\* p.adjusted  $\leq 0.01$ , \*\*\* p.adjusted  $\leq 0.001$ ,  $n = 4$ ). PRINT IN COLOR.

metabolic pathways, especially TCA Cycle and Fatty Acid  $\beta$ -oxidation, but downregulated pathways associated with the ECM and proliferation from day 8 on. The parent compounds also displayed upregulation of metabolic pathways like TCA Cycle and Fatty Acid  $\beta$ -oxidation but showed an upregulation of proliferation-related pathways, except for 10  $\mu$ M DINP which indicated downregulation of these pathways (Fig. 4B). 10 nM and 10  $\mu$ M OH-MPHP induced fewer changes than MHNP and MINCH, but also showed downregulation of ECM- and proliferation-associated pathways.

Furthermore, transcriptional upstream regulators, which may be linked to the given protein abundance changes and biological processes, as well as associated diseases and functions were found enriched via IPA (Fig. 4C). Enriched upstream regulators for rosiglitazone induced differentiation included PPARG (PPAR $\gamma$ ) itself as well as PPARGC1A (peroxisome proliferator-activated receptor gamma coactivator 1-alpha), LIPE (hormone-sensitive lipase), and LEP (leptin), which are PPAR $\gamma$  coactivators or target genes (Fig. 4C). SCD (stearoyl-CoA desaturase) is involved in the production of unsaturated fatty acids, and the downregulation of Wnt signaling, whose decrease is necessary for adipocyte differentiation (Sinner et al., 2012; Wang et al., 2005). MINCH showed significant enrichment for PPARGC1A, PPARG, and LIPE at 10  $\mu$ M and to a far lesser extent at 10 nM. 10  $\mu$ M MHNP revealed significant enrichment for PPARGC1A and SCD but was below significance for PPARG and LEP. The 10 nM concentration of MHNP seemed to slightly impact SCD, PPARGC1A, and LEP.

Enrichment of IPA diseases and functions revealed mechanisms associated with lipid production and fat tissue expansion for 10  $\mu$ M MINCH and MHNP (Fig. 4C). Notably, for some of these mechanisms there was a trend for rosiglitazone as well that did not reach significance.

To gain deeper insights into the compounds' modes of action and identify proteins that are central players of the induced effects (key drivers), a weighted gene correlation network analysis (WGCNA) was performed. Using the  $\text{Log}_2(\text{FC})$ s obtained by proteomic analysis, co-

abundant proteins were clustered into seven modules labeled by colors and correlated with compound treatments (Supplement 1, Fig. S5). Modules green and yellow showed the highest and most significant correlations and were, hence, used for further analysis. In the green module, 10  $\mu$ M MINCH and MHNP as well as rosiglitazone showed the highest significance with positive correlation, followed by lower correlation induced by 10  $\mu$ M of OH-MPHP, DPHP, and 10 nM DPHP (Fig. 5A). 10 nM of the metabolites led to a significant negative correlation with the green module, whereas DINP and 10 nM of DINCH seemed to have no significant impact on this module.

For the yellow module, the 10  $\mu$ M concentration of MINCH, MHNP, and rosiglitazone showed a highly negative correlation (Fig. 5A). 10  $\mu$ M of DPHP, OH-MPHP, DINCH, and DNP displayed a slight but significant negative correlation with the yellow module, while 10 nM of DNP and MHNP showed a slight positive correlation to this module, and the other treatments caused no changes.

Next, proteins driving the observed correlations (key drivers), being highly relevant for the induced effects, were determined based on gene significances and module memberships (Fig. 5B, cutoff 0.7). This comparably stringent cutoff led to the identification of key drivers for only the most highly correlated treatments: rosiglitazone and 10  $\mu$ M of metabolites. The key drivers were subjected to KEGG enrichment to identify associated biological functions. The green module contained key drivers involved in metabolism, such as the citrate cycle, fatty acid production, and PPAR signaling (Fig. 5C). The yellow module was dominated by proteins related to cytoskeleton and extracellular matrix (Fig. 5D).

The top 10 key drivers based on summed module membership and gene significance were determined next for the green and the yellow module for each treatment (Fig. 5E). The candidates of the green module showed a substantial increase in abundance over time for rosiglitazone and similarly for 10  $\mu$ M MINCH and MHNP. For 10  $\mu$ M of OH-MPHP, only some key drivers, such as FABP4, FASN, ACYL, FABP5, and GPD1, were increased during differentiation. The top 10 key drivers

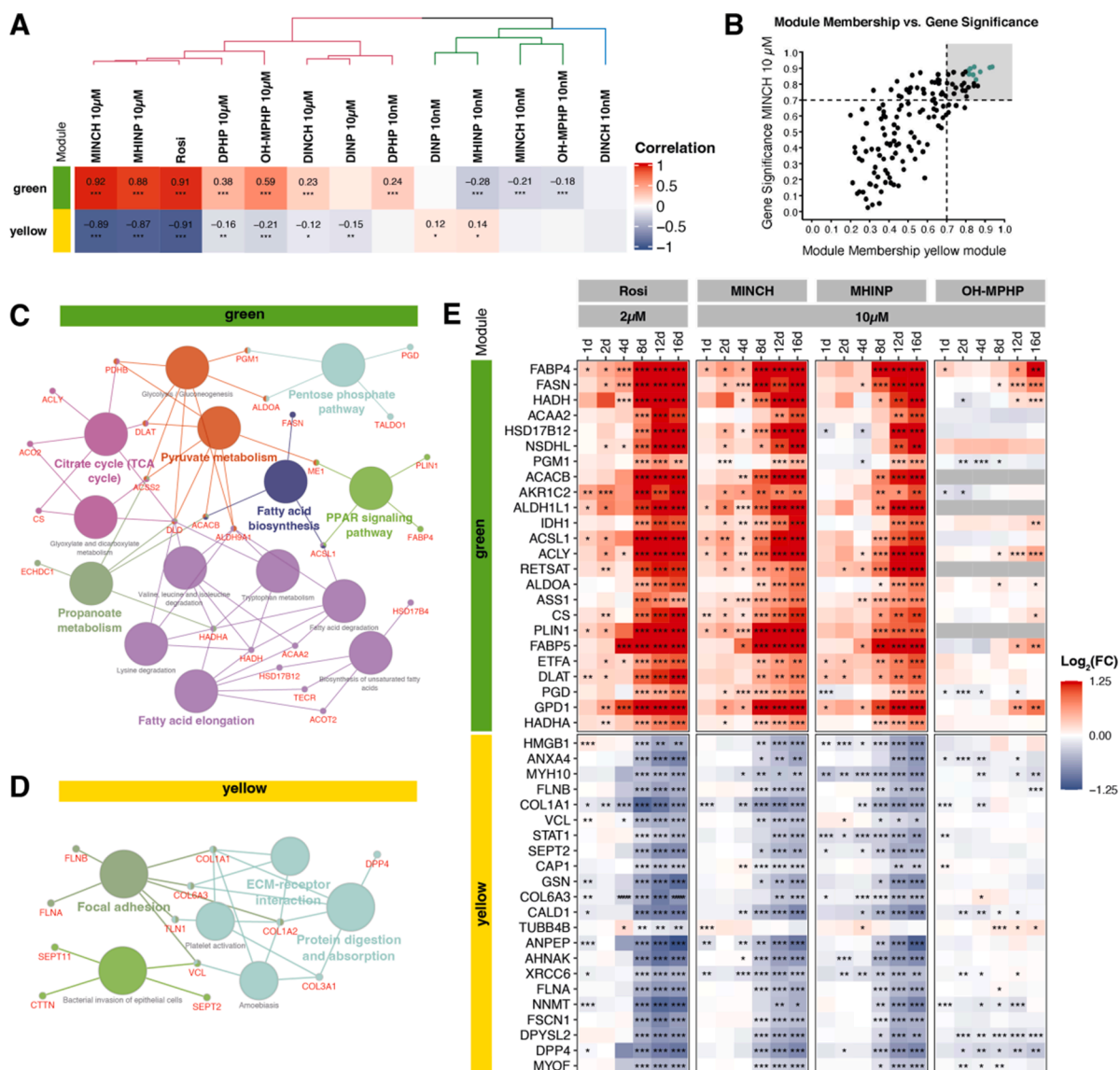


**Fig. 5.** WGCNA of proteomics data from SGBS preadipocytes exposed to selected plasticizers. (A) Correlation between selected modules of co-abundant proteins and treatments indicated by color. The significance of the correlation is indicated with asterisks (\*  $p \leq 0.05$ , \*\*  $p \leq 0.01$ , \*\*\*  $p \leq 0.001$ ). (B) Key drivers of a module were obtained using a stringent 0.7 cutoff for gene significance and module membership and resulted in key drivers for only rosiglitazone and the metabolites at 10  $\mu\text{M}$  (MINCH 10  $\mu\text{M}$  displayed as example). Selection is marked by the grey area. The top 10 key drivers are labeled as green points. (C) KEGG enrichment for the key drivers from the green module. (D) KEGG enrichment for key drivers from the yellow module. (E) Heatmap of combined top 10 key drivers per treatment based on summed module membership and gene significance. Significant changes are labeled with asterisks (\*  $p \leq 0.05$ , \*\*  $p \leq 0.01$ , \*\*\*  $p \leq 0.001$ ,  $n = 4$ ). PRINT IN COLOR.

such as DPP4, COL1A1, COL1A2, COL3A1, FLNA, and FLNB of the yellow module showed a decrease over time, which again was strongest for rosiglitazone, 10  $\mu\text{M}$  MINCH, and 10  $\mu\text{M}$  MHINP, and only slightly decreased for some candidates involved in remodeling of the cytoskeleton (e.g. DPYSL2, DPP4, ANXA4, and CALD1) upon treatment with 10  $\mu\text{M}$  OH-MPHP. The changes were most pronounced starting at day 8 of differentiation (Fig. 5E). Interestingly, some key drivers showed similar changes for the parent plasticizers (Supplement 1, Fig. S7). The green module key drivers PLIN1, FABP4, FABP5, and FASN were predominantly increased for both plasticizer concentrations and the abundance of those key drivers was remarkably higher in 10 nM plasticizer treatments compared to 10 nM metabolite treatments, which showed only very slight changes (Supplement 1, Fig. S7). KEGG enrichment of key drivers revealed involvement of PPAR signaling as a driving mechanism (Fig. 5C). Upon closer inspection of common PPAR targets ('PPARgene Database'), increased abundances for both, PPAR $\gamma$ - and PPAR $\alpha$ -targets,

were observed in treatments with the plasticizer metabolites as well as with rosiglitazone (Supplement 1, Fig. S6).

In summary, the plasticizer metabolites at 10  $\mu\text{M}$  highly increased metabolism and pathways associated with adipogenesis while down-regulating pathways associated with the ECM, both via related upstream regulators, reflecting the induction of adipocyte differentiation similar to rosiglitazone.

### 3.2.3. Adverse effects on mature adipocytes

Besides understanding plasticizer effects during the differentiation of preadipocytes, assessing effects on mature adipocytes is essential for evaluating impacts on preexisting adipose tissue. Therefore, SGBS adipocytes were differentiated according to the standard differentiation protocol, which includes exposure to rosiglitazone from day 0 to day 4 resulting in mature adipocytes on day 12 (Fig. 2). These differentiated, mature adipocytes were exposed to the plasticizers or their metabolites

from day 12 to day 20 and analyzed on the last day. Interestingly, lipid content was mostly decreased by DINCH, MINCH, DPHP, and OH-MPHP (Fig. 6A). It was unchanged by DINP and MHINP, with a slight increase for 1 μM MHINP. In accordance with the results obtained in SGBS pre-adipocytes (Fig. 3A), only 100 μM of MINCH led to a decrease in cell viability of >20% (Supplement 1, Fig. S8).

Secretion of adipokines leptin, MCP-1, and adiponectin was significantly increased by all 10 μM treatments and in tendency for the 10 nM treatments (Fig. 6B). Adiponectin secretion was significantly decreased by all treatments (Fig. 6B).

To summarize, chronic exposure of mature adipocytes to the selected

plasticizers or their metabolites for 8 days decreased lipid content for four of six compounds while not having a relevant impact on cell viability with the exception of 100 μM MINCH. Furthermore, all compounds significantly induced secretion of the adipokines leptin, MCP-1, and adiponectin release.

### 3.2.4. Proteomic analysis of exposed mature adipocytes

To gain insights into the mode of action of the plasticizers in mature adipocytes, as well as the source of the observed effects, proteomic analysis was conducted on day 20.

The compounds induced substantial changes in the numbers of

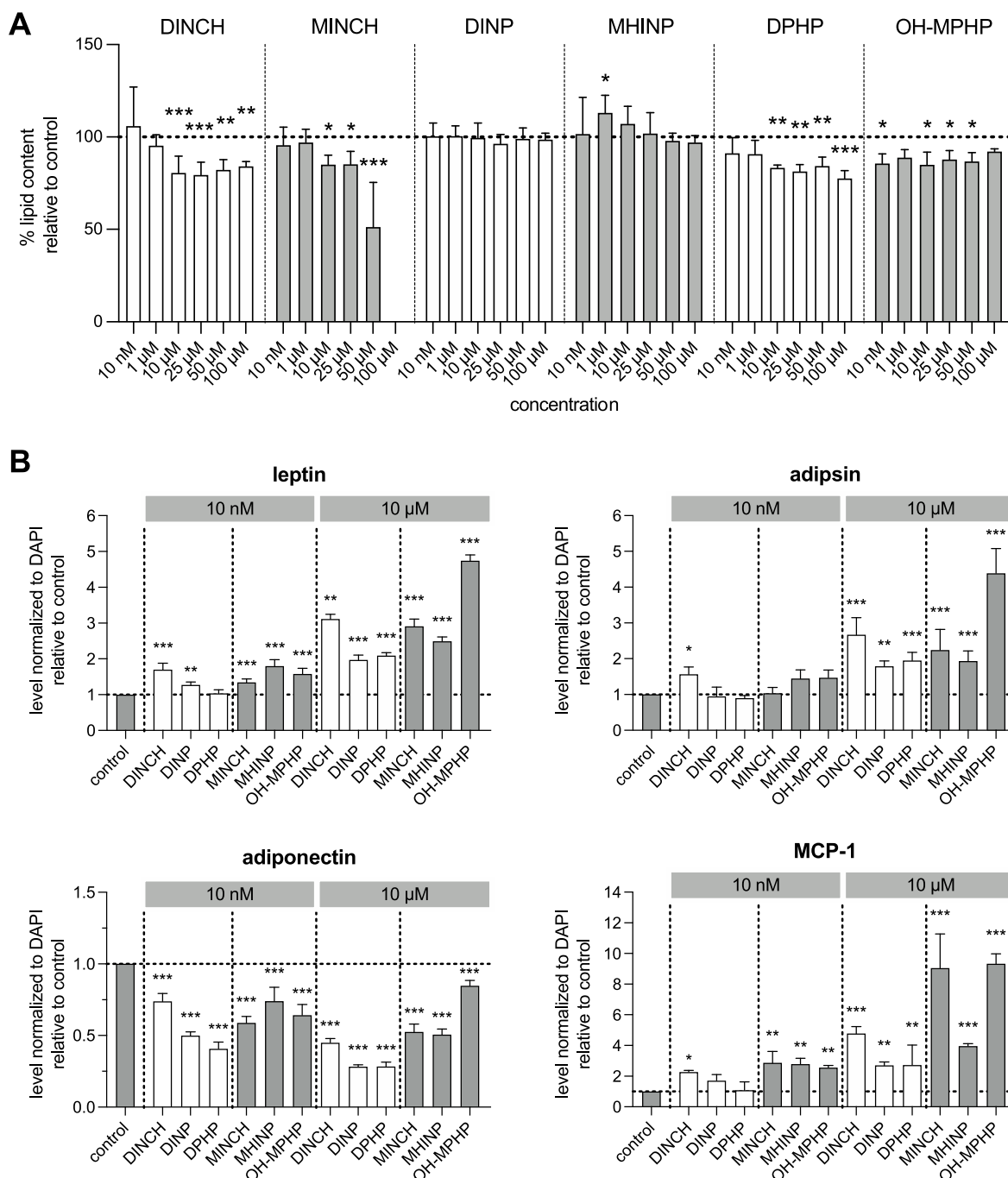


**Fig. 6.** Effect of selected plasticizers and their metabolites on lipid accumulation and adipokine release in mature adipocytes. Mature SGBS adipocytes were exposed to the compounds for 8 days starting from day 12 after differentiation start. (A) Lipid accumulation relative to undifferentiated vehicle control was quantified on day 20 and normalized to DAPI staining of DNA content. (B) Levels of adipokines leptin, MCP-1, adiponectin, and adiponectin relative to the vehicle control in cell supernatants on day 20. Significant changes are labeled with asterisks (\*  $p \leq 0.05$ , \*\*  $p \leq 0.01$ , \*\*\*  $p \leq 0.001$ ,  $n = 4$ ).

significantly altered proteins compared to the vehicle control (0.01% MeOH v/v), which were stronger for the higher concentration of 10  $\mu$ M (Fig. 7A). The top 10 affected signaling pathways unraveled using IPA included ECM and cytoskeleton-related pathways, which were upregulated by all the compounds compared to the control (Fig. 7B). Metabolic pathways including Oxidative Phosphorylation, TCA Cycle, Fatty Acid  $\beta$ -oxidation, and amino acid degradation pathways were downregulated by all the compounds. Interestingly, the top 10 regulated pathways also included NRF2-mediated Oxidative Stress Response and Ferroptosis Signaling Pathway, which were upregulated by the compounds. In general, the differences between low and high concentrations were higher than the differences between the compounds, which showed similar effects overall (Fig. 7A, B).

Enrichment of IPA diseases and functions revealed mechanisms associated with lipolysis for most of the plasticizer and metabolite treatments (Fig. 7C).

To analyze the underlying cause of the observed plasticizer effects in detail, a WGCNA was again performed according to the analysis during adipogenesis. Using  $\text{Log}_2(\text{FC})$ s of treatment vs. vehicle control, six modules were obtained that were correlated to the compound treatments (Supplement 1, Fig. S9). The modules turquoise and blue displayed the strongest correlation and significance (Fig. 8A). From those modules, key drivers were selected using a 0.7 cutoff of module

membership and gene significance (Fig. 8B). A KEGG enrichment of these key drivers revealed mostly metabolic pathways for the blue module, including Oxidative Phosphorylation, TCA Cycle, fatty acid synthesis processes, amino acid degradation, and PPAR signaling (Fig. 8C). Accordingly, we observed a decrease of PPAR $\gamma$  targets by all plasticizer and metabolite treatments (Supplement 1, Fig. S10). For the turquoise module, most enriched proteins belonged to the ECM or focal adhesion processes, which are macromolecular assemblies linked to the ECM (Fig. 8C). Additionally, the turquoise module contained proteins of Glutathione metabolism, including glutathione peroxidases and glutamine synthesis (PKM, GLS), which is a precursor of glutathione (Fig. 8C). As before, also the top 10 key drivers based on summed module membership and gene significance were considered. The top 10 key drivers unraveled for the different treatments in the blue module were downregulated upon all treatment but appeared to be stronger downregulated for the high concentration (Fig. 8E). The combined top 10 key drivers of the turquoise module were generally upregulated for all compounds, and, again, this effect was more pronounced for the high concentration (Fig. 8E).

Since KEGG enrichment of the blue module revealed Glutathione Metabolism (Fig. 8C) and the top 10 regulated pathways included NRF2-mediated Oxidative Stress Response as well as Ferroptosis Signaling (Fig. 7B), proteins involved in oxidative stress and lipid peroxidation

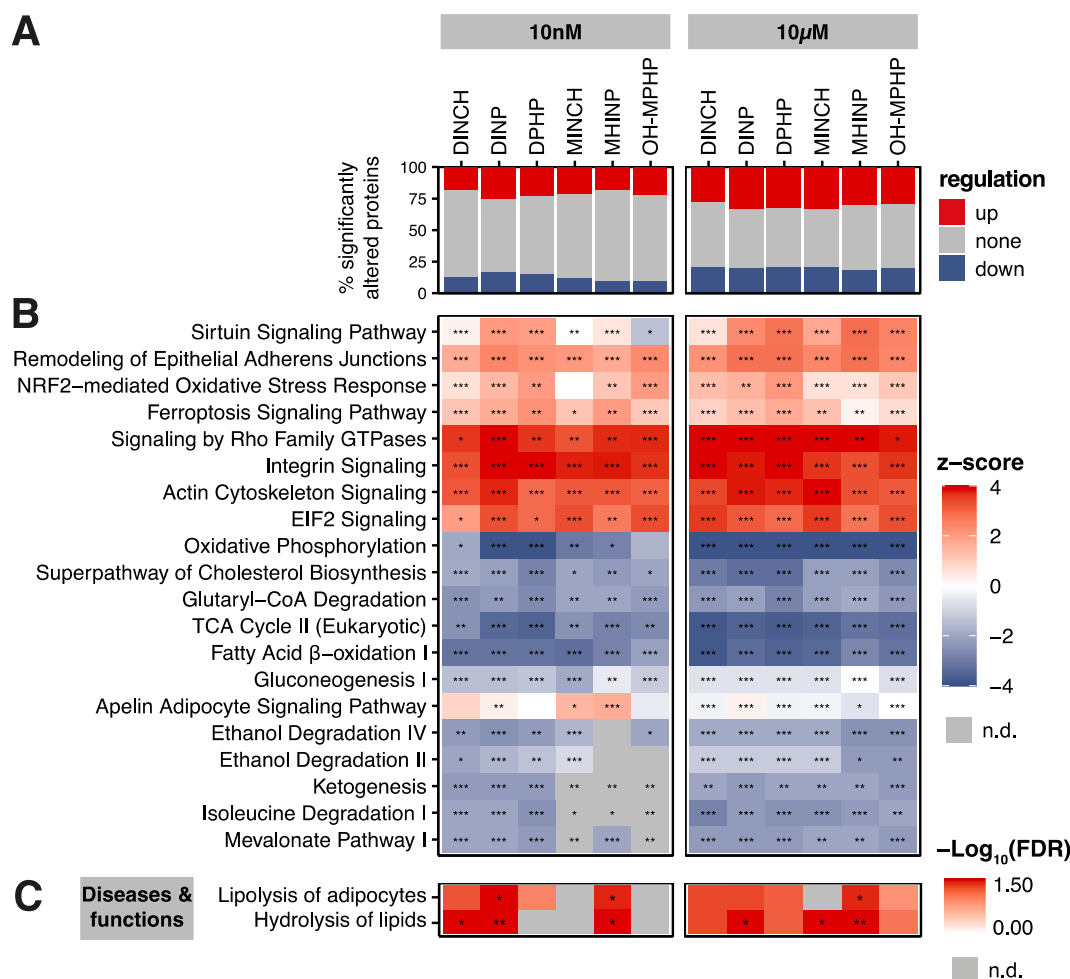


**Fig. 7. Proteomics analysis of mature SGBS adipocytes exposed to plasticizers and their metabolites for 8 days.** Displayed are results obtained by comparison of treatment vs. vehicle control (0.01% MeOH, v/v) on day 8 post differentiation. (A) Percentage of significantly altered proteins ( $p \leq 0.05$ ,  $n = 4$ ). (B) Selection of top 10 pathways obtained via Ingenuity Pathways Analysis (IPA) for the different treatments. The heatmap colors are based on z-scores calculated by IPA, indicating the direction of pathway regulation (z-score  $> 0$  upregulated pathway, z-score  $< 0$  downregulated, grey represents z-score not available). (C) Diseases and functions were enriched via IPA. The level of enrichment is visualized based on the adjusted p-value. Significant changes of pathways and diseases and functions are indicated with asterisks (\* p.adjusted  $\leq 0.05$ , \*\* p.adjusted  $\leq 0.01$ , \*\*\* p.adjusted  $\leq 0.001$ ,  $n = 4$ ). PRINT IN COLOR.



## 4. Discussion

### 4.1. Plasticizer metabolites act through activation of PPAR $\gamma$ in human adipocytes

Two processes enable the expansion of adipose tissue: The differentiation of new adipocytes from adipocyte progenitor cells (hyperplasia) and an increase in size of existing differentiated adipocytes due to increased lipid accumulation (hypertrophy) (Rosen and Spiegelman, 2014). While both mechanisms contribute to the development of obesity, especially the latter is associated with adipose tissue dysfunction and metabolic diseases.

Preadipocyte differentiation into mature, lipid-storing adipocytes is primarily regulated by the transcription factor PPAR $\gamma$  (Rosen et al., 1999). Using SPR and the cell-based GeneBLAzer<sup>®</sup> PPAR $\gamma$  bioassay, we previously demonstrated that DEHP itself does not interact with PPAR $\gamma$ , while its metabolites MEHP and MEOHP bind and activate it (Kratochvil et al., 2018). Using this setup, we now screened 20 plasticizers for PPAR $\gamma$  interactions. We found several plasticizers being able to bind to the PPAR $\gamma$  LBD. Most of the binders were metabolites, with the exception of DIBP and BBP (Fig. 1). The DINCH metabolite MINCH showed the strongest binding to PPAR $\gamma$ , comparable to the efficacy of the natural ligand 15d-PGJ2. Not all PPAR $\gamma$ -binding compounds were able to activate it in the bioassay, possibly because they are not capable of passing the cell membrane or inducing a conformational change that results in activation. Antagonistic effects may be possible but we did not observe a suppression of basal PPAR $\gamma$  activity (Supplement 1, Fig. S3), nor did we test the compounds in the presence of e.g. rosiglitazone. Counterintuitively, some compounds did not bind but activated PPAR $\gamma$ , suggesting that not all possible interactions can be identified using SPR. As the PPAR $\gamma$  LBD is immobilized on the surface of the sensor chip, flexibility is limited, which may prevent some PPAR $\gamma$ -ligand interactions. Additionally, some compounds that activated PPAR $\gamma$  but had no adipogenic effect in SGBS cells may be not potent enough at the applied concentrations or induce insufficient conformational changes, recruitment of transcriptional cofactors, and subsequent binding of ligand-specific PPAR response elements (PPREs) on the DNA.

Nonetheless, all compounds that induced adipogenesis and lipid accumulation in human SGBS preadipocytes also activated PPAR $\gamma$  in the reporter gene assay, with the exception of DIBP and MINCH (Fig. 1). For MINCH, activation of PPAR $\gamma$ , as well as PPAR $\alpha$ , was previously shown by Engel et al. (2018) at  $\mu$ M-concentrations. While we used the commercially available PPAR $\gamma$ -UAS-bla HEK293 cell assay, they transfected HEK293 cells with a PPAR $\gamma$  plasmid (Engel et al., 2018), which may lead to different results. Additionally, Campioli et al. (2015) have observed induction of adipogenesis and lipid accumulation in rat adipocytes by MINCH that could be blocked by a PPAR $\alpha$ -antagonist and to a lesser extent using a PPAR $\gamma$ -antagonist. Therefore, they suspected MINCH as a potent PPAR $\alpha$  agonist, but did not rule out an interaction with PPAR $\gamma$ . PPAR $\alpha$  agonists have also been reported to induce lipid accumulation and adipogenesis in SGBS cells, although to a lesser extent than rosiglitazone (Arnesen et al., 2019). PPAR $\beta/\delta$ , on the other hand, mostly regulates fatty acid oxidation and is not able to independently induce adipogenesis (Brun et al., 1996). A reliable measure of PPAR activity is the comparison of PPAR-specific targets, directly regulated by the transcription factors. Both, the plasticizer metabolites and the PPAR $\gamma$ -specific agonist rosiglitazone increased PPAR $\gamma$ - and PPAR $\alpha$ -targets in SGBS cells (Supplement 1, Fig. S6), suggesting synergistic activity of the two receptors. Moreover, given the structural similarities of the two PPAR isoforms and that PPAR ligands can often activate more than one isoform, it is possible that the plasticizer metabolites interact with both, PPAR $\gamma$  and PPAR $\alpha$ . Thus, while we demonstrated the interaction of several compounds with PPAR $\gamma$ , including MHINP, OH-MPHP, and possibly MINCH, a potential interaction with PPAR $\alpha$  may be investigated in further studies. Moreover, interactions with other nuclear receptors, which have not been investigated here, cannot be excluded.

Taken together, we found several compounds to interact with PPAR $\gamma$  with a subsequent induction of lipid accumulation in human preadipocytes for some of them. MINCH, MHINP, and OH-MPHP exerted the highest adipogenic potential and for MHINP and OH-MPHP we were able to clearly demonstrate direct binding and activation of PPAR $\gamma$  as an underlying mechanism.

### 4.2. Plasticizer metabolites induce adipogenesis similar to rosiglitazone

Investigations of adipogenic properties of plasticizers have previously been primarily conducted in murine 3T3-L1 cells and were mostly focused on the DEHP metabolite MEHP. While the parent plasticizer DEHP appears to have no significant effect on adipogenesis, MEHP increases lipid accumulation and adipogenesis via PPAR $\gamma$ -activation in 3T3-L1 cells (Feige et al., 2007; Hao et al., 2012; Hurst and Waxman, 2003; Qi et al., 2019). Moreover, Feige et al. (2007) observed a similar selective activation of PPAR $\gamma$  target genes and the recruitment of specific PPAR $\gamma$  coactivators as for rosiglitazone.

Our findings suggest comparable adipogenic properties for the metabolites of the emerging DEHP substitutes DINCH, DINP, and DPHP. We demonstrated that MINCH, MHINP, and OH-MPHP induce adipocyte differentiation, with the DINCH-metabolite MINCH having the highest potency (Fig. 1, Fig. 3B). Its potency is similar to the DEHP metabolite MEHP which showed an increase in lipid accumulation and adipogenesis, described for other cell lines, also in our SGBS cells (Supplement 1, Fig. S4). The induction of lipid accumulation by the plasticizer metabolites and rosiglitazone was reflected by enhanced ECM remodeling in order to increase lipid storage capacities at the beginning of differentiation (Fig. 4B) (Mariman and Wang, 2010). In accordance with the literature, an adipogenesis-promoting effect in rat and mouse adipocytes was previously observed for the DINCH-metabolite MINCH (Campioli et al., 2015).

Nonetheless, proteomics analysis revealed that also the parent compounds cause an increase of the identified key drivers, which are key adipogenesis markers such as FABP4, FASN, PLIN1, and ACYL (Supplement 1, Fig. S7) (Moseti et al., 2016). The increase was apparent for both concentrations, with the lower concentration showing a higher increase of adipogenesis markers by the parent compounds than the metabolites, suggesting more than a metabolite-induced effect after metabolization in the cells. Since the parent compounds showed neither binding nor activation of PPAR $\gamma$ , their subtle effect on the induction of adipogenesis-marker increase seems to be regulated otherwise.

Interestingly, the plasticizer metabolites enhanced cell viability in a concentration-dependent manner (Fig. 3A), which was also observed in rosiglitazone-differentiated cells (Fig. 3A), suggesting a proliferative effect. Preadipocytes, including SGBS cells (Felicidade et al., 2018), undergo so-called "mitotic clonal expansion" (MCE) at the onset of differentiation, in which growth-arrested preadipocytes re-enter the cell cycle and complete approximately two rounds of proliferation before entering a transcriptional cascade that eventually leads to mature adipocytes (Merkestein et al., 2015). The fat mass- and obesity-associated (FTO) gene which affects early adipogenesis by regulating MCE, is located downstream of PPAR $\gamma$  and can be induced by PPAR $\gamma$  agonists (Zhang et al., 2015). Thus, the observed proliferative effect of the metabolites above 10  $\mu$ M and rosiglitazone (Fig. 3A) may indicate an induction of MCE mediated by PPAR $\gamma$  activation.

Moreover, adipokine secretion was impaired by the plasticizers and their metabolites (Fig. 3C). Due to the increased adipogenesis, secretion of the PPAR $\gamma$  target leptin was increased by 10  $\mu$ M of MINCH, MHINP, and OH-MPHP, even higher than by rosiglitazone. While leptin levels correlate with the body fat mass, it functions as a negative feedback signal of energy homeostasis (Harris, 2014). Nonetheless, chronically increased leptin concentrations are associated with obesity and can lead to leptin resistance, which further accelerates overeating and obesity (Harris, 2014). It needs to be evaluated *in vivo* whether this may also be a consequence of the plasticizer exposure. Furthermore, adipsin was

reported to be increased in obese individuals and was linked to a heightened prevalence of metabolic syndrome (Wang, Zheng, et al. 2020). The increase in adiponin by DINCH, DINP, and their metabolites may therefore accelerate a prevalence for both. The pro-inflammatory adipokine MCP-1 mediates the infiltration of macrophages into the adipose tissue and, thus, contributes to inflammation and results in insulin resistance (Sartipy and Loskutoff, 2003). Like rosiglitazone, the plasticizers and metabolites seem to decrease MCP-1 secretion in preadipocytes.

However, our data suggest that the plasticizer metabolites exert their adipogenic properties rather at low  $\mu\text{M}$  than at nM concentrations. Whether these concentrations are physiologically relevant in the adipose tissue remains to be evaluated, but they can certainly contribute to mixture effects. Phthalate concentrations in human serum and urine range from low to mid nM concentrations (Katsikantami et al., 2016; Specht et al., 2014; Wang et al., 2019; Zettergren et al., 2021). Yet, exposure in the adipose tissue might be even higher due to bioaccumulation of the hydrophobic compounds and may increase specifically under conditions of increased lipolysis, but reliable data on adipose tissue concentrations is lacking. Additionally, it needs to be considered that an even longer continuous exposure period or an additive effect of plasticizer mixtures may increase the adipogenic potential.

Interestingly, urinary metabolites of DINP including MHINP, which showed strong adipogenic potential in our study, have recently been associated with elevated BMIs in Swedish children and young adults (Zettergren et al., 2021). While both hyperplasia and hypertrophy are contributing factors to adipose tissue expansion and obesity in adults, hyperplastic processes play a much more critical role in children's adipose tissue and hyperplasia is significantly increased in obese children (Landgraf et al., 2015), potentially making them more susceptible to adipogenic compounds facilitating or accelerating adipose tissue expansion. Obese children have a 90% chance of being overweight as adolescents (Geserick et al., 2018) and the early onset of overweight and obesity in children is a determining factor for co-morbidities in adulthood (Korner et al., 2007; Vukovic et al., 2019; Ward et al., 2017).

In summary, the plasticizer metabolites of MINCH and MHINP show a strong induction of adipogenic markers, pathways, and adipokine secretion at 10  $\mu\text{M}$ , similar to rosiglitazone. Nonetheless, the parent compounds DINCH, DINP, and DPHP seem to already induce some adipogenesis key drivers at 10 nM, indicating an unknown PPAR $\gamma$ - and biotransformation-unrelated mechanism.

#### 4.3. Plasticizers and their metabolites cause adipocyte dysfunction in mature adipocytes

Investigation of the plasticizer effects on mature adipocytes have so far been neglected, although hypertrophy of the adipose tissue is a key factor contributing to obesity and co-morbidities (Hammarstedt et al., 2018). Therefore, we investigated the exposure of mature adipocytes to the plasticizers and their metabolites and demonstrated that DINCH, DINP, and DPHP, as well as MINCH, MHINP, and OH-MPHP all affected and altered adipocyte function. Contrary to what we observed in the preadipocytes, parent compounds and metabolites exhibited a similar degree and direction of pathway regulation in mature adipocytes, which were already prominent at 10 nM, but more pronounced at 10  $\mu\text{M}$  (Fig. 7B). Moreover, DINCH, MINCH, DPHP, and OH-MPHP decreased lipid content (Fig. 6A) and PPAR $\gamma$  targets (Supplement 1, Fig. S10) compared to the vehicle control. Interestingly, thiazolidinediones (TZDs) such as rosiglitazone were reported to decrease lipid content by 10% when added to mature adipocytes and induced changes in PPAR $\gamma$  target gene regulation opposite to those during adipogenesis, similar to what we observed for the plasticizers and their metabolites, indicating a different modulation of PPAR $\gamma$  activity in differentiated adipocytes (Wang et al., 2007; Wilson-Fritch et al., 2004). Instead, TZDs enhanced fatty acid degradation pathways such as fatty acid- $\beta$  oxidation, TCA cycle, and oxidative phosphorylation. As fatty acid degradation

processes were downregulated by the plasticizers and metabolites (Fig. 7B, Fig. 8C, E), this indicates increased lipolysis, which was significantly enriched in the pathway analysis (Fig. 7C). The release of fatty acids ultimately may lead to ectopic lipid deposition *in vivo* (Hammarstedt et al., 2018).

In line with reduced lipid content, the compounds strongly enhanced ECM-associated and focal adhesion proteins, which were among the top key drivers (Fig. 8D) and reflect the morphological changes. Similarly, increased ECM and cytoskeleton remodeling with reduced oxidative phosphorylation, and altered metabolic mechanisms were previously observed in adipocytes as a result of a high-fat diet (HFD) (Jones et al., 2020). Adipocyte ECM flexibility is vital for a healthy expansion and metabolic flexibility of the adipose tissue (Hammarstedt et al., 2018). An ECM that is too rigid and inflexible limits lipid storage capacity and expansion of the adipocyte, resulting in inflammation and ectopic deposition of lipids, as well as induction of stress-pathways, and death of adipocytes (Sun et al., 2013). Moreover, excessive build-up of ECM also leads to adipose tissue fibrosis, which has been linked to decreased insulin sensitivity and a decreased ability for weight loss in the case of subcutaneous adipose tissue fibrosis (Divoux et al., 2010; Lawler et al., 2016).

Furthermore, upregulation of the NRF2-mediated stress response indicated the cellular response to elevated reactive oxygen species (ROS) (Fig. 7B). The Nuclear Factor Erythroid 2-related Factor 2 (NRF2) is activated as an initial response to oxidative stress, inducing the expression of antioxidants (Vnukov et al., 2017). Moreover, key driver analysis revealed increased intensities of proteins of the glutathione metabolism (Fig. 8E), which plays a vital role in the antioxidant defense (Wu et al., 2004). The enhanced key driver GPX4 is directly involved in the neutralization of lipid peroxidation products (Yant et al., 2003), suggesting that excessive plasticizer-induced ROS production may have led to lipid peroxidation. Excessive lipid peroxidation in adipocytes can not only lead to damaging of cell membrane and organelles but also to ferroptosis, which is an iron-dependent, regulated cell death that is strongly accelerated by redox imbalance and lipid oxidation products (Hao et al., 2018). While the mechanisms behind lipid peroxidation leading to ferroptosis remains unclear (Liu et al., 2020), growing evidence links ferroptosis to cardiovascular diseases and inflammation (Yu et al., 2021). Although investigation of cell viability by DAPI staining did not indicate a relevant decrease at the tested concentrations of 10 nM and 10  $\mu\text{M}$ , increased ferroptosis signaling (Fig. 7B) may suggest that the tested exposure already induced this process and cellular defense mechanisms via GPX4, as observed in the key driver analysis (Fig. 8D, E), may prevent substantial ferroptosis and subsequent cell death. Interestingly, urinary phthalate metabolite levels of phthalates DEHP, DBP, and DIBP have been associated with oxidative stress biomarkers in women's urine (Ferguson et al., 2015). Supporting this observation, our results suggest an imbalance in redox homeostasis resulting in the observed adipocyte cellular responses to counteract oxidative stress and lipid peroxidation induced by the plasticizers and their metabolites in mature adipocytes.

Previously, Fernando et al. (2020) showed that oxidative stress in adipocytes leads to mitochondrial dysfunction and subsequent impairment of metabolic processes, promoting insulin resistance. This is in accordance with the decreased oxidative phosphorylation and impaired metabolic processes we found in mature adipocytes after exposure to the plasticizers and their metabolites. Reflecting adipocyte dysfunction, the plasticizers altered adipokine secretion patterns with significantly increased leptin, adiponin, and MCP-1 secretion (Fig. 6B). Furthermore, adiponectin secretion was decreased, linking plasticizers and their metabolites to adipose tissue inflammation and insulin resistance (Krieg et al., 2020; Ziemke and Mantzoros, 2010). Exposure of mice to DEHP also resulted in significant weight gain and reduced adiponectin serum levels (Klötting et al., 2015), strengthening the hypothesis for pathological consequences of a plasticizer-mediated decrease of adiponectin-secretion.

Notably, the parent plasticizers, which showed no PPAR $\gamma$  interaction and a neglectable adipogenic effect in preadipocytes, had the same effects as the metabolites in mature adipocytes. Either this suggests an unspecific stress-induced mechanism of action rather than a PPAR $\gamma$ -mediated one, or an overlap of both mechanisms. Additionally, increased levels of lipases in mature adipocytes may facilitate more effective metabolization of plasticizers (Frederiksen et al., 2007), thus increasing metabolite-mediated effects.

Moreover, since the plasticizers and their metabolite induced oxidative stress in mature adipocytes, this raises the question if part of the adipogenesis promoting effect is mediated by increased ROS production (de Villiers et al., 2018). However, no substantial increase in oxidative stress response pathways or antioxidants was observed in preadipocytes. Additionally, since the parent plasticizers and the metabolites exerted comparable levels of oxidative stress responses in mature adipocytes, a ROS-mediated induction of adipogenesis would not explain the significantly stronger effects of the plasticizer metabolites. Whether increased ROS production by plasticizers plays a role in adipogenesis induction needs to be determined in further studies.

In light of these results, future studies on the adipogenic effects of xenobiotics could provide deeper insights into the modes of action in adipose tissue by including mature adipocytes and performing kinetic studies on dynamic changes.

In summary, the plasticizers and their metabolites appear to induce oxidative stress and mitochondrial dysfunction in mature adipocytes at low concentrations, causing altered lipid metabolism and release, with an increase in ECM remodeling, upregulation of ferroptosis signaling, and proinflammatory and insulin resistance promoting adipokine secretion.

## 5. Conclusion

We showed that a variety of plasticizers or their metabolites bind to

and activate PPAR $\gamma$ , resulting in the induction of adipogenesis in human preadipocytes. DINCH, DINP, and DPHP metabolites displayed the most potent adipogenic properties by inducing adipogenesis and enhancing associated markers similarly to the PPAR $\gamma$ -agonist rosiglitazone (Fig. 9). In mature adipocytes, DINCH, DINP, DPHP, and their metabolites disturbed lipid storage, caused oxidative stress, impaired metabolic homeostasis, and altered adipokine release linked to inflammation and insulin resistance (Fig. 9). Based on the observed adverse effects and similarities to known high fat diet-induced adipose tissue impairment, exposure to plasticizers and their metabolites might result in an increase of fat mass, dysregulation of adipose tissue function, inflammation, and enhanced risk for metabolic syndrome (Fig. 9).

In conclusion, given the similarity of their obesogenic mechanisms compared to the restricted DEHP, we can clearly conclude that DINCH, DINP, and DPHP are unsuitable replacements.

## Funding

This research was funded by the German Federal Environmental Foundation (DBU) as a personal fellowship of Alexandra Schaffert. Furthermore, we are grateful for support by the UFZ-funded platform *ProMetheus* for proteome and metabolome analysis. Matthias Blüher, John T. Heiker, Martin von Bergen, Katharina Walter, and Josi Arnold are thankful for funding by the German Research Foundation (DFG) for the Clinical Research Center "Obesity Mechanisms" SFB 1052/3 (B1, C7, Z3). The reporter gene experiments were performed using the platform CITEPro (Chemicals in the Environment Profiler) funded by the Helmholtz Association with co-funding by the States of Saxony and Saxony-Anhalt.

## CRediT authorship contribution statement

**Alexandra Schaffert:** Conceptualization, Data curation,

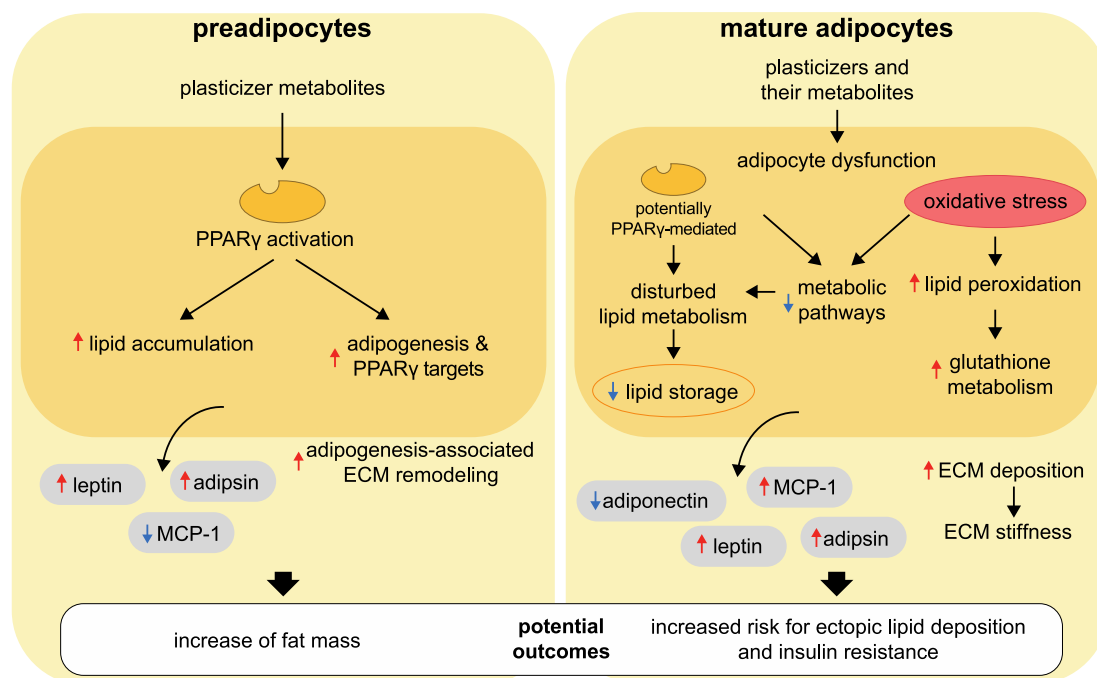


**Fig. 9.** Proposed mode of action of the tested plasticizers and metabolites in human adipocytes. In preadipocytes, the metabolites induced differentiation and enhanced lipid accumulation via PPAR $\gamma$ -activation, while remodeling the ECM allowing for growth. The metabolites elevated leptin and adipsin secretion but decreased the pro-inflammatory MCP-1. These effects may lead to an increase in fat mass. In mature adipocytes, the parent plasticizers and metabolites caused adipocyte dysfunction with impaired lipid metabolism and storage, impaired metabolic homeostasis, increased ECM remodeling, and altered adipokine release linked to inflammation and insulin resistance. The compounds induced oxidative stress as well as lipid peroxidation and enhanced glutathione metabolism as an anti-oxidative response. These effects are similar to HFD-induced adipocyte changes and may increase the risk for ectopic lipid deposition and insulin resistance. PRINT IN COLOR.

Methodology, Investigation, Validation, Writing – original draft, Visualization, Project administration. **Isabel Karkossa:** Data curation, Supervision, Writing – review & editing. **Elke Ueberham:** Resources, Supervision, Writing – review & editing. **Rita Schlichting:** Methodology, Investigation, Visualization, Writing – review & editing. **Katharina Walter:** Investigation. **Josi Arnold:** Investigation. **Matthias Blüher:** Writing – review & editing. **John T. Heiker:** Writing – review & editing. **Jörg Lehmann:** Resources, Writing – review & editing. **Martin Wabitsch:** Resources. **Beate I. Escher:** Resources, Project administration, Writing – review & editing. **Martin von Bergen:** Supervision, Writing – review & editing, Project administration. **Kristin Schubert:** Conceptualization, Supervision, Writing – review & editing, Project administration.

## Declaration of Competing Interest

The authors declare that they have no known competing financial interests or personal relationships that could have appeared to influence the work reported in this paper.

## Appendix A. Supplementary data

Supplementary data to this article can be found online at <https://doi.org/10.1016/j.envint.2022.107279>.

## References

- Abdelal, M., le Roux, C.W., Docherty, N.G., 2017. Morbidity and mortality associated with obesity. *Ann. Transl. Med.* 5, 161.
- Aldridge, A., Kouroupis, D., Churchman, S., English, A., Ingham, E., Jones, E., 2013. Assay validation for the assessment of adipogenesis of multipotential stromal cells—a direct comparison of four different methods. *Cytotherapy* 15, 89–101.
- Arnesen, H., Haj-Yasein, N.N., Tungen, J.E., Soedling, H., Matthews, J., Paulsen, S.M., Nebb, H.I., Sylte, I., Hansen, T.V., Saether, T., 2019. Molecular modelling, synthesis, and biological evaluations of a 3,5-disubstituted isoxazole fatty acid analogue as a PPARalpha-selective agonist. *Bioorg. Med. Chem.* 27, 4059–4068.
- Bannusch, A., Karkossa, I., Buhs, S., Nollau, P., Kettler, K., Balas, M., Dinischiotu, A., Hellack, B., Wiemann, M., Luch, A., von Bergen, M., Haase, A., Schubert, K., 2020. A multi-omics approach reveals mechanisms of nanomaterial toxicity and structure-activity relationships in alveolar macrophages. *Nanotoxicology* 14, 181–195.
- Benjamin, S., Masai, E., Kamimura, N., Takahashi, K., Anderson, R.C., Faisal, P.A., 2017. Phthalates impact human health: Epidemiological evidences and plausible mechanism of action. *J. Hazard. Mater.* 340, 360–383.
- Brun, R.P., Tontonoz, P., Forman, B.M., Ellis, R., Chen, J., Evans, R.M., Spiegelman, B.M., 1996. Differential activation of adipogenesis by multiple PPAR isoforms. *Genes Dev.* 10, 974–984.
- Campoli, E., Duong, T.B., Deschamps, F., Papadopoulos, V., 2015. Cyclohexane-1,2-dicarboxylic acid diisononyl ester and metabolite effects on rat epididymal stromal vascular fraction differentiation of adipose tissue. *Environ. Res.* 140, 145–156.
- 'The Consumer Product Safety Improvement Act (CPSIA)'. US Consumer Product Safety Commission Accessed 10 January 2022. <https://www.cpsc.gov/Regulations-Laws-Standards/Statutes/The-Consumer-Product-Safety-Improvement-Act>.
- Darbre, P.D., 2017. Endocrine Disruptors and Obesity. *Curr. Obes. Rep.* 6, 18–27.
- de Villiers, D., Potgieter, M., Ambele, M.A., Adam, L., Durandt, C., Pepper, M.S., 2018. The Role of Reactive Oxygen Species in Adipogenic Differentiation. *Adv. Exp. Med. Biol.* 1083, 125–144.
- Divoux, A., Tordjman, J., Lacasa, D., Veyrie, N., Hugol, D., Aissat, A., Basdevant, A., Guerre-Millo, M., Poitou, C., Zucker, J.D., Bedossa, P., Clement, K., 2010. Fibrosis in human adipose tissue: composition, distribution, and link with lipid metabolism and fat mass loss. *Diabetes* 59, 2817–2825.
- Dragulescu, A.; Arendt, C. 2020. "xlxs: Read, Write, Format Excel 2007 and Excel 97/2000/XP/2003 Files." In.
- ECHA, European Chemicals Agency. 2018. 'ANNEX XVII TO REACH – Conditions of restriction', Entry 51.
- Engel, A., Buhrike, T., Kasper, S., Behr, A.C., Braeuning, A., Jessel, S., Seidel, A., Volkel, W., Lampen, A., 2018. The urinary metabolites of DINCH(RI) have an impact on the activities of the human nuclear receptors ERalpha, ERbeta, AR, PPARalpha and PPARgamma. *Toxicol. Lett.* 287, 83–91.
- EP, European Parliament and the council of the european union. 2006. 'REGULATION (EC) No 1907/2006 OF THE EUROPEAN PARLIAMENT AND OF THE COUNCIL of 18 December 2006 concerning the Registration, Evaluation, Authorisation and Restriction of Chemicals (REACH), establishing a European Chemicals Agency, amending Directive 1999/45/EC and repealing Council Regulation (EEC) No 793/93 and Commission Regulation (EC) No 1488/94 as well as Council Directive 76/769/EEC and Commission Directives 91/155/EEC, 93/67/EEC, 93/105/EC and 2000/21/EC', *Official Journal of the European Union*, L 396: 1-849.
- Escher, B.I., Glauch, L., König, M., Mayer, P., Schlichting, R., 2019. Baseline Toxicity and Volatility Cutoff in Reporter Gene Assays Used for High-Throughput Screening. *Chem. Res. Toxicol.* 32, 1646–1655.
- Feige, J.N., Gelman, L., Rossi, D., Zoete, V., Metivier, R., Tudor, C., Anghel, S.I., Grosdidier, A., Lathion, C., Engelborghs, Y., Michielin, O., Wahli, W., Desvergne, B., 2007. The endocrine disruptor monoethyl-hexyl-phthalate is a selective peroxisome proliferator-activated receptor gamma modulator that promotes adipogenesis. *J. Biol. Chem.* 282, 19152–19166.
- Felicidade, I., Sartori, D., Coort, S.L.M., Semperebon, S.C., Niwa, A.M., D'Epiro, G.F.R., Biazzi, B.I., Marques, L.A., Evelo, C.T., Mantovani, M.S., Ribeiro, L.R., 2018. Role of 1alpha,25-Dihydroxyvitamin D3 in Adipogenesis of SGBS Cells: New Insights into Human Preadipocyte Proliferation. *Cell. Physiol. Biochem.* 48, 397–408.
- Ferguson, K.K., McElrath, T.F., Chen, Y.H., Mukherjee, B., Meeke, J.D., 2015. Urinary phthalate metabolites and biomarkers of oxidative stress in pregnant women: a repeated measures analysis. *Environ. Health Perspect.* 123, 210–216.
- Fernando, R., Wardelmann, K., Deubel, S., Kehm, R., Jung, T., Mariotti, M., Vasilaki, A., Gladyshev, V.N., Kleinriders, A., Grune, T., Castro, J.P., 2020. Low steady-state oxidative stress inhibits adipogenesis by altering mitochondrial dynamics and decreasing cellular respiration. *Redox Biol.* 32, 101507.
- Fischer-Posovszky, P., Newell, F.S., Wabitsch, M., Tornqvist, H.E., 2008. Human SGBS Cells – a Unique Tool for Studies of Human Fat Cell Biology. *Obesity Facts* 1, 184–189.
- Frederiksen, H., Skakkebaek, N.E., Andersson, A.M., 2007. Metabolism of phthalates in humans. *Mol. Nutr. Food Res.* 51, 899–911.
- Geserick, M., Vogel, M., Gausche, R., Lipek, T., Spielau, U., Keller, E., Pfaffle, R., Kiess, W., Korner, A., 2018. Acceleration of BMI in Early Childhood and Risk of Sustained Obesity. *N. Engl. J. Med.* 379, 1303–1312.
- Graffelman, J., van Eeuwijk, F., 2005. Calibration of multivariate scatter plots for exploratory analysis of relations within and between sets of variables in genomic research. *R package version 1 (7)*, 5.
- Gu, Z., Gu, L., Eils, R., Schlesner, M., Brors, B., 2014. circlize Implements and enhances circular visualization in R. *Bioinformatics* 30, 2811–2812.
- Hahladakis, J.N., Velis, C.A., Weber, R., Iacovidou, E., Purnell, P., 2018. An overview of chemical additives present in plastics: Migration, release, fate and environmental impact during their use, disposal and recycling. *J. Hazard. Mater.* 344, 179–199.
- Hammarstedt, A., Gogg, S., Hedjazifar, S., Nerstedt, A., Smith, U., 2018. Impaired Adipogenesis and Dysfunctional Adipose Tissue in Human Hypertrophic Obesity. *Physiol. Rev.* 98, 1911–1941.
- Hao, C., Cheng, X., Xia, H., Ma, X., 2012. The endocrine disruptor mono-(2-ethylhexyl) phthalate promotes adipocyte differentiation and induces obesity in mice. *Biosci. Rep.* 32, 619–629.
- Hao, S., Liang, B., Huang, Q., Dong, S., Wu, Z., He, W., Shi, M., 2018. Metabolic networks in ferroptosis. *Oncol. Lett.* 15, 5405–5411.
- Harris, R.B., 2014. Direct and indirect effects of leptin on adipocyte metabolism. *BBA* 1842, 414–423.
- Hoffstedt, J., Arvidsson, E., Sjolín, E., Wahlen, K., Arner, P., 2004. Adipose tissue adiponectin production and adiponectin serum concentration in human obesity and insulin resistance. *J. Clin. Endocrinol. Metab.* 89, 1391–1396.
- Hogberg, J., Hanberg, A., Berglund, M., Skerfving, S., Remberger, M., Calafat, A.M., Filipsson, A.F., Jansson, B., Johansson, N., Appelgren, M., Hakansson, H., 2008. Phthalate diesters and their metabolites in human breast milk, blood or serum, and urine as biomarkers of exposure in vulnerable populations. *Environ. Health Perspect.* 116, 334–339.
- Hughes, C.S., Foehr, S., Garfield, D.A., Furlong, E.E., Steinmetz, L.M., Krijgsvelde, J., 2014. Ultrasensitive proteome analysis using paramagnetic bead technology. *Mol. Syst. Biol.* 10, 757.
- Hughes, C.S., Moggridge, S., Müller, T., Sorensen, P.H., Morin, G.B., Krijgsvelde, J., 2019. Single-pot, solid-phase-enhanced sample preparation for proteomics experiments. *Nat. Protoc.* 14, 68–85.
- Hurst, C.H., Waxman, D.J., 2003. Activation of PPARalpha and PPARgamma by environmental phthalate monoesters. *Toxicol. Sci.* 74, 297–308.
- Jones, J.E.C., Rabhi, N., Orofino, J., Gaminí, R., Perissi, V., Vernochet, C., Farmer, S.R., 2020. The Adipocyte Acquires a Fibroblast-Like Transcriptional Signature in Response to a High Fat Diet. *Sci. Rep.* 10, 2380.
- Katsikantami, I., Sifakis, S., Tzatzarakis, M.N., Vakonaki, E., Kalantzi, O.I., Tsatsakis, A. M., Rizos, A.K., 2016. A global assessment of phthalates burden and related links to health effects. *Environ. Int.* 97, 212–236.
- Klötting, N., Hesselbarth, N., Gericke, M., Kunath, A., Biemann, R., Chakaroun, R., Kosacka, J., Kovacs, P., Kern, M., Stumvoll, M., Fischer, B., Rolle-Kampczyk, U., Feltens, R., Otto, W., Wissenbach, D.K., von Bergen, M., Blüher, M., 2015. Di-(2-Ethylhexyl)-Phthalate (DEHP) Causes Impaired Adipocyte Function and Alters Serum Metabolites. *PLoS ONE* 10, e0143190.
- König, M., Escher, B.I., Neale, P.A., Krauss, M., Hilscherová, K., Novák, J., Teodorović, I., Schulze, T., Seidensticker, S., Kamal Hashmi, M.A., Ahlheim, J., Brack, W., 2017. Impact of untreated wastewater on a major European river evaluated with a combination of in vitro bioassays and chemical analysis. *Environ. Pollut.* 220, 1220–1230.
- Korner, A., Kratzsch, J., Gausche, R., Schaab, M., Erbs, S., Kiess, W., 2007. New predictors of the metabolic syndrome in children—role of adipocytokines. *Pediatr. Res.* 61, 640–645.
- Kratochvil, I., Hofmann, T., Rother, S., Schlichting, R., Moretti, R., Scharnweber, D., Hintze, V., Escher, B.I., Meiler, J., Kalkhof, S., von Bergen, M., 2018. Mono(2-ethylhexyl) phthalate (MEHP) and mono(2-ethyl-5-oxohexyl) phthalate (MEOHP) but not di(2-ethylhexyl) phthalate (DEHP) bind productively to the peroxisome proliferator-activated receptor gamma. *Rapid Commun. Mass Spectrom.*

- Krieg, L., Schaffert, A., Kern, M., Landgraf, K., Wabitsch, M., Beck-Sickinger, A.G., Koerner, A., Blüher, M., von Bergen, M., Schubert, K., 2020. An MRM-Based Multiplexed Quantification Assay for Human Adipokines and Apolipoproteins. *Molecules (Basel, Switzerland)* 25, 775.
- Landgraf, K., Rockstroh, D., Wagner, I.V., Weise, S., Tauscher, R., Schwartz, J.T., Löffler, D., Buhlig, U., Wojan, M., Till, H., Kratzsch, J., Kiess, W., Blüher, M., Korner, A., 2015. Evidence of early alterations in adipose tissue biology and function and its association with obesity-related inflammation and insulin resistance in children. *Diabetes* 64, 1249–1261.
- Langfelder, P., Horvath, S., 2008. WGCNA: An R package for weighted correlation network analysis. *BMC Bioinform.* 9, 559.
- Langfelder, P., Horvath, S., 2012. Fast R Functions For Robust Correlations And Hierarchical Clustering. *J. Stat. Softw.* 46.
- Lawler, H.M., Underkofler, C.M., Kern, P.A., Erickson, C., Bredbeck, B., Rasouli, N., 2016. Adipose Tissue Hypoxia, Inflammation, and Fibrosis in Obese Insulin-Sensitive and Obese Insulin-Resistant Subjects. *J. Clin. Endocrinol. Metab.* 101, 1422–1428.
- Le Magueresse-Battistoni, B., Labaronne, E., Vidal, H., Naville, D., 2017. Endocrine disrupting chemicals in mixture and obesity, diabetes and related metabolic disorders. *World J. Biol. Chem.* 8, 108–119.
- Lefterova, M.L., Haakonsson, A.K., Lazar, M.A., Mandrup, S., 2014. PPARgamma and the global map of adipogenesis and beyond. *Trends Endocrinol. Metab.* 25, 293–302.
- Lind, P.M., Zethelius, B., Lind, L., 2012. Circulating Levels of Phthalate Metabolites Are Associated With Prevalent Diabetes in the Elderly. *Diabetes Care* 35, 1519–1524.
- Liu, J., Zhang, C., Wang, J., Wenwei, H., Feng, Z., 2020. The Regulation of Ferroptosis by Tumor Suppressor p53 and its Pathway. *Int. J. Mol. Sci.* 21.
- Mahto, A., 2019. splitstackshape: Stack and Reshape Datasets After Splitting Concatenated Values. R package version 1 (4), 8.
- Mariman, E.C., Wang, P., 2010. Adipocyte extracellular matrix composition, dynamics and role in obesity. *Cell. Mol. Life Sci.* 67, 1277–1292.
- Merkstein, Myrte, Samantha Laber, Fiona McMurray, Daniel Andrew, Gregor Sachse, Jeremy Sanderson, Mengdi Li, Samuel Usher, Dyan Sellayah, Frances M. Ashcroft, and Roger D. Cox. 2015. 'FTO influences adipogenesis by regulating mitotic clonal expansion', *Nature Communications*, 6.
- Moseti, D., Regassa, A., Kim, W.K., 2016. Molecular Regulation of Adipogenesis and Potential Anti-Adipogenic Bioactive Molecules. *Int. J. Mol. Sci.* 17.
- Muscogiuri, G., Barrea, L., Laudisio, D., Savastano, S., Colao, A., 2017. Obesogenic endocrine disruptors and obesity: myths and truths. *Arch. Toxicol.* 91, 3469–3475.
- Nagorka, R., Koschorreck, J., 2020. Trends for plasticizers in German freshwater environments - Evidence for the substitution of DEHP with emerging phthalate and non-phthalate alternatives. *Environ. Pollut.* 262, 114237.
- Neels, J.G., Grimaldi, P.A., 2014. Physiological functions of peroxisome proliferator-activated receptor beta. *Physiol. Rev.* 94, 795–858.
- Perez-Riverol, Y., Csordas, A., Bai, J., Bernal-Llinares, M., Hewapathirana, S., Kundu, D. J., Inuganti, A., Griss, J., Mayer, G., Eisenacher, M., Pérez, X., Audkoreit, J., Pfeuffer, J., Sachsenberg, T., Yilmaz, S., Tiwary, S., Cox, J., Audain, E., Walzer, M., Jarmuzak, A.F., Ternent, T., Brazma, A., Vizcaíno, J.A., 2019. The PRIDE database and related tools and resources in 2019: improving support for quantification data. *Nucleic Acids Res.* 47, D442–D450.
- 'PPARGene: Database of PPAR target genes'. <http://www.ppargene.org/downloads.php>.
- Qi, W., Zhou, L., Zhao, T., Ding, S., Xu, Q., Han, X., Zhao, Y., Song, X., Zhao, T., Zhang, X., Ye, L., 2019. Effect of the TYK-2/STAT-3 pathway on lipid accumulation induced by mono-2-ethylhexyl phthalate. *Mol. Cell. Endocrinol.* 484, 52–58.
- Ribeiro, C.M., Beserra, B.T.S., Silva, N.G., Lima, C.L., Rocha, P.R.S., Coelho, M.S., Neves, F.A.R., Amato, A.A., 2020. Exposure to endocrine-disrupting chemicals and anthropometric measures of obesity: a systematic review and meta-analysis. *BMJ Open* 10, e033509.
- Rosen, E.D., Spiegelman, B.M., 2014. What we talk about when we talk about fat. *Cell* 156, 20–44.
- Rosen, E.D., Sarraf, P., Troy, A.E., Bradwin, G., Moore, K., Milstone, D.S., Spiegelman, B. M., Mortensen, R.M., 1999. PPARγ Is Required for the Differentiation of Adipose Tissue In Vivo and In Vitro. *Mol. Cell* 4, 611–617.
- Sartipy, P., Loskutoff, D.J., 2003. Monocyte chemoattractant protein 1 in obesity and insulin resistance. *Proc. Natl. Acad. Sci. U. S. A.* 100, 7265–7270.
- Schaedlich, K., Gebauer, S., Hunger, L., Beier, L.S., Koch, H.M., Wabitsch, M., Fischer, B., Ernst, J., 2018. DEHP deregulates adipokine levels and impairs fatty acid storage in human SGBS-adipocytes. *Sci. Rep.* 8, 3447.
- Schaffert, A., Arnold, J., Karkossa, I., Blüher, M., von Bergen, M., Schubert, K., 2021a. The Emerging Plasticizer Alternative DINCH and Its Metabolite MINCH Induce Oxidative Stress and Enhance Inflammatory Responses in Human THP-1 Macrophages. *Cells* 10.
- Schaffert, A., Krieg, L., Weiner, J., Schlichting, R., Ueberham, E., Karkossa, I., Bauer, M., Landgraf, K., Junge, K.M., Wabitsch, M., Lehmann, J., Escher, B.I., Zenclussen, A.C., Korner, A., Blüher, M., Heiker, J.T., von Bergen, M., Schubert, K., 2021b. Alternatives for the worse: Molecular insights into adverse effects of bisphenol a and substitutes during human adipocyte differentiation. *Environ. Int.* 156, 106730.
- Schmidt, J.S., Schaedlich, K., Fiandanese, N., Pocar, P., Fischer, B., 2012. Effects of di(2-ethylhexyl) phthalate (DEHP) on female fertility and adipogenesis in C3H/N mice. *Environ. Health Perspect.* 120, 1123–1129.
- Shang, J., Kojetin, D.J., 2021. Structural mechanism underlying ligand binding and activation of PPARγ. *Structure*.
- Silva, M.J., Samandar, E., Preau Jr., J.L., Reidy, J.A., Needham, L.L., Calafat, A.M., 2007. Quantification of 22 phthalate metabolites in human urine. *J. Chromatogr. B Analyt. Technol. Biomed. Life Sci.* 860, 106–112.
- Sinner, D.I., Kim, G.J., Henderson, G.C., Igal, R.A., 2012. StearoylCoA desaturase-5: a novel regulator of neuronal cell proliferation and differentiation. *PLoS ONE* 7, e39787.
- Specht, I.O., Toft, G., Hougaard, K.S., Lindh, C.H., Lenters, V., Jonsson, B.A., Heederik, D., Giwercman, A., Bonde, J.P., 2014. Associations between serum phthalates and biomarkers of reproductive function in 589 adult men. *Environ. Int.* 66, 146–156.
- Spieß, A., N., 2018. qPCR: Modelling and Analysis of Real-Time PCR Data. In *R package version 1.4-1*.
- Stahlhut, R.W., van Wijngaarden, E., Dye, T.D., Cook, S., Swan, S.H., 2007. Concentrations of urinary phthalate metabolites are associated with increased waist circumference and insulin resistance in adult U.S. males. *Environ. Health Perspect.* 115, 876–882.
- Sun, K., Tordjman, J., Clement, K., Scherer, P.E., 2013. Fibrosis and adipose tissue dysfunction. *Cell Metab.* 18, 470–477.
- Turner, S., 2019. Tmisc: Turner Miscellaneous. In *R package version (1)*, 22.
- van Marrewijk, L.M., Polyak, S.W., Hijnen, M., Kuruvilla, D., Chang, M.R., Shin, Y., Kamenecka, T.M., Griffin, P.R., Bruning, J.B., 2016. SR2067 Reveals a Unique Kinetic and Structural Signature for PPARgamma Partial Agonism. *ACS Chem. Biol.* 11, 273–283.
- Van Vliet, E.D., Reitano, E.M., Chhabra, J.S., Bergen, G.P., Whyatt, R.M., 2011. A review of alternatives to di (2-ethylhexyl) phthalate-containing medical devices in the neonatal intensive care unit. *J. Perinatol.* 31, 551–560.
- Vnukov, V.V., Gutsenko, O.I., Milyutina, N.P., Kornienko, I.V., Ananyan, A.A., Plotnikov, A.A., Panina, S.B., 2017. SkQ1 Regulates Expression of Nrf2, ARE-Controlled Genes Encoding Antioxidant Enzymes, and Their Activity in Cerebral Cortex under Oxidative Stress. *Biochemistry (Mosc)* 82, 942–952.
- Vukovic, R., Dos Santos, T.J., Ybarra, M., Atar, M., 2019. Children With Metabolically Healthy Obesity: A Review. *Front. Endocrinol. (Lausanne)* 10, 865.
- Wabitsch, M., Brenner, R.E., Melzner, I., Braun, M., Moller, P., Heinze, E., Debatin, K.M., Hauner, H., 2001. Characterization of a human preadipocyte cell strain with high capacity for adipose differentiation. *Int. J. Obes. Relat. Metab. Disord.* 25, 8–15.
- Wang, J., Yu, L., Schmidt, R.E., Su, C., Huang, X., Gould, K., Cao, G., 2005. Characterization of HSCD5, a novel human stearoyl-CoA desaturase unique to primates. *Biochem. Biophys. Res. Commun.* 332, 735–742.
- Wang, P., Renes, J., Bouwman, F., Bunschoten, A., Mariman, E., Keijer, J., 2007. Absence of an adipogenic effect of rosiglitazone on mature 3T3-L1 adipocytes: increase of lipid catabolism and reduction of adipokine expression. *Diabetologia* 50, 654–665.
- Wang, Y., Zheng, X., Xie, X., Qian, W., Ren, Z., Chen, Y., Wu, X., Liao, K., Ren, W., 2020a. Body fat distribution and circulating adipin are related to metabolic risks in adult patients with newly diagnosed growth hormone deficiency and improve after treatment. *Biomed. Pharmacother.* 132, 110875.
- Wang, Y., Zhu, H., Kannan, K., 2019. A Review of Biomonitoring of Phthalate Exposures. *Toxics* 7.
- Wang, Z., Karkossa, I., Grosskopf, H., Rolle-Kampczyk, U., Hacker Müller, J., von Bergen, M., Schubert, K., 2020b. Comparison of quantitation methods in proteomics to define relevant toxicological information on AhR activation of HepG2 cells by BaP. *Toxicology* 152652.
- Ward, Z.J., Long, M.W., Resch, S.C., Giles, C.M., Craddock, A.L., Gortmaker, S.L., 2017. Simulation of Growth Trajectories of Childhood Obesity into Adulthood. *N. Engl. J. Med.* 377, 2145–2153.
- Wickham, H., 2007. Reshaping Data with the reshapePackage. *J. Stat. Softw.* 21.
- Wickham, H., 2011. The Split-Apply-Combine Strategy for Data Analysis. *J. Stat. Softw.* 40.
- Wickham, H., 2016. ggplot2: Elegant Graphics for Data Analysis. Springer-Verlag, New York.
- Wickham, H., 2019. tidy: Tidy Messy Data. R package version 1.
- Wickham, H., Bryan, J., 2019. readxl: Read Excel Files. R package version 1 (3), 1.
- Wilson-Fritch, L., Nicoloso, S., Chouinard, M., Lazar, M.A., Chui, P.C., Leszyk, J., Straubhaar, J., Czech, M.P., Corvera, S., 2004. Mitochondrial remodeling in adipose tissue associated with obesity and treatment with rosiglitazone. *J. Clin. Invest.* 114, 1281–1289.
- Wu, G., Fang, Y.Z., Yang, S., Lupton, J.R., Turner, N.D., 2004. Glutathione metabolism and its implications for health. *J. Nutr.* 134, 489–492.
- Xiao, N., 2018. ggsci: Scientific Journal and Sci-Fi Themed Color Palettes for 'ggplot2'. R package version 2, 9.
- Xie, H., Han, W., Xie, Q., Xu, T., Zhu, M., Chen, J., 2022. Face mask-A potential source of phthalate exposure for human. *J. Hazard. Mater.* 422, 126848.
- Yant, L.J., Ran, Q., Rao, L., Van Remmen, H., Shibatani, T., Belter, J.G., Motta, L., Richardson, A., Prolla, T.A., 2003. The selenoprotein GPX4 is essential for mouse development and protects from radiation and oxidative damage insults. *Free Radical Biol. Med.* 34, 496–502.
- Yu, C., Chen, L., Luo, H., Chen, J., Cheng, F., Gui, C., Zhang, R., Shen, J., Chen, K., Jiang, H., Shen, X., 2004. Binding analyses between Human PPARgamma-LBD and ligands. Surface plasmon resonance biosensor correlating with circular dichroic spectroscopy determination and molecular docking. *Eur. J. Biochem.* 271, 386–397.
- Yu, Y., Yan, Y., Niu, F., Wang, Y., Chen, X., Su, G., Liu, Y., Zhao, X., Qian, L., Liu, P., Xiong, Y., 2021. Ferroptosis: a cell death connecting oxidative stress, inflammation and cardiovascular diseases. *Cell Death Discov.* 7, 193.
- Zettergren, A., Andersson, N., Larsson, K., Kull, I., Melen, E., Georgelis, A., Berglund, M., Lindh, C., Bergstrom, A., 2021. Exposure to environmental phthalates during preschool age and obesity from childhood to young adulthood. *Environ. Res.* 192, 110249.

Zhang, M., Zhang, Y., Ma, J., Guo, F., Cao, Q., Zhang, Y., Zhou, B., Chai, J., Zhao, W., Zhao, R., 2015. The Demethylase Activity of FTO (Fat Mass and Obesity Associated Protein) Is Required for Preadipocyte Differentiation. *PLoS ONE* 10, e0133788.

Zhang, X., Smits, A.H., van Tilburg, G.B., Ovaa, H., Huber, W., Vermeulen, M., 2018. Proteome-wide identification of ubiquitin interactions using UbiA-MS. *Nat. Protoc.* 13, 530–550.

Ziemke, F., Mantzoros, C.S., 2010. Adiponectin in insulin resistance: lessons from translational research. *Am. J. Clin. Nutr.* 91, 258S–261S.